

AWARD NUMBER: W81XWH-15-1-0256

TITLE: Determine the Dynamic Response to Androgen Blockade Therapy in Circulating Tumor Cells of CRPC Patients by Transcription-based Reporter Vectors

PRINCIPAL INVESTIGATOR: Wu, Lily

CONTRACTING ORGANIZATION: University of California, Los Angeles
Los Angeles, CA 90095-1406

REPORT DATE: NOVEMBER 2019

TYPE OF REPORT: Final Report

PREPARED FOR: U.S. Army Medical Research and Materiel Command
Fort Detrick, Maryland 21702-5012

DISTRIBUTION STATEMENT: Approved for Public Release; Distribution Unlimited

The views, opinions and/or findings contained in this report are those of the author(s) and should not be construed as an official Department of the Army position, policy or decision unless so designated by other documentation.

REPORT DOCUMENTATION PAGE

Form Approved
OMB No. 0704-0188

Public reporting burden for this collection of information is estimated to average 1 hour per response, including the time for reviewing instructions, searching existing data sources, gathering and maintaining the data needed, and completing and reviewing this collection of information. Send comments regarding this burden estimate or any other aspect of this collection of information, including suggestions for reducing this burden to Department of Defense, Washington Headquarters Services, Directorate for Information Operations and Reports (0704-0188), 1215 Jefferson Davis Highway, Suite 1204, Arlington, VA 22202-4302. Respondents should be aware that notwithstanding any other provision of law, no person shall be subject to any penalty for failing to comply with a collection of information if it does not display a currently valid OMB control number. **PLEASE DO NOT RETURN YOUR FORM TO THE ABOVE ADDRESS.**

1. REPORT DATE NOVEMBER 2019		2. REPORT TYPE Annual		3. DATES COVERED 1 August 2015- 31 July 2019	
4. TITLE AND SUBTITLE Determine the Dynamic Response to Androgen Blockade Therapy in Circulating Tumor Cells of CRPC Patients by Transcription-based Reporter Vectors				5a. CONTRACT NUMBER W81XWH-15-1-0256	
				5b. GRANT NUMBER	
				5c. PROGRAM ELEMENT NUMBER	
6. AUTHOR(S) Wu, Lily E-Mail: lwu@mednet.ucla.edu				5d. PROJECT NUMBER	
				5e. TASK NUMBER	
				5f. WORK UNIT NUMBER	
7. PERFORMING ORGANIZATION NAME(S) AND ADDRESS(ES) UNIVERSITY OF CALIFORNIA, LOS ANGELES 11000 KINROSS AVENUE, STE 102 LOS ANGELES, CA 90095				8. PERFORMING ORGANIZATION REPORT NUMBER	
9. SPONSORING / MONITORING AGENCY NAME(S) AND ADDRESS(ES) U.S. Army Medical Research and Materiel Command Fort Detrick, Maryland 21702-5012				10. SPONSOR/MONITOR'S ACRONYM(S)	
				11. SPONSOR/MONITOR'S REPORT NUMBER(S)	
12. DISTRIBUTION / AVAILABILITY STATEMENT Approved for Public Release; Distribution Unlimited					
13. SUPPLEMENTARY NOTES					
14. ABSTRACT Circulating tumor cells (CTCs) are tumor cells that are shed into the blood stream by a solid tumor such as prostate cancer. Current data supports CTCs likely denote the more aggressive tumor cells that have metastatic potential. It is extremely challenging to identify CTCs in context of 10 ⁸ excess white blood cells in peripheral blood. The use of advanced microfluidic chip-based CTC detection method, such as the "Nano-Velcro" chip used in this project, has been shown to exhibit greatly enhanced CTC capture efficiency in prostate cancer patients, providing an earlier and more sensitive readout of treatment response than the FDA approved CellSearch™ CTC detection method, serum PSA or radiographic CT assessment. However, a limitation of the current detection technology is its inability to assess dynamic functional activity, such as the AR pathway, in the living CTCs as the immunohistochemistry approach of current methods can only provide static protein expression in the CTCs. This DOD funded project aims to incorporate the use of AR-driven reporter recombinant vectors to query dynamic AR functional status in viable CTCs captured by the Nano-Velcro chip.					
15. SUBJECT TERMS Prostate Cancer, Circulating Tumor Cells, Prostate-specific Adenoviral vectors, PSA, PSES					
16. SECURITY CLASSIFICATION OF:			17. LIMITATION OF ABSTRACT	18. NUMBER OF PAGES	19a. NAME OF RESPONSIBLE PERSON
a. REPORT	b. ABSTRACT	c. THIS PAGE			USAMRMC
Unclassified	Unclassified	Unclassified	Unclassified	31	19b. TELEPHONE NUMBER (include area code)

Table of Contents

Cover	1
SF 298	2
Table of Contents	3
Introduction	4
Body	4-7
Key Research Accomplishments	7-8
Reportable Outcomes	8
Conclusions	8
References	9
Appendix	10-31

Introduction

Analyses from prostate cancer patients so far indicated that circulating tumor cells (CTCs) represent an easily accessible liquid biopsy to assess the aggressive, metastatic tumor cells, as the number of CTCs is much higher in advanced, metastatic disease (1, 2). However, the detection of CTCs is hampered by their extreme low numbers amongst the great excess of red and white blood cells. To increase the certainty of detecting prostate cancer cells and its AR functional status, an important clinical drug response factor, we proposed to use an adenoviral mediated reporter gene transfer into cells in peripheral blood. The adenoviral vector will express green fluorescent protein driven by an amplified PSA or an amplified PSMA promoter, which are both prostate tissue-specific that is AR- or non AR-responsive, respectively. Thus, any nucleated cell in the circulation that expresses GFP should be a prostate cancer cell. Due to personnel and change of expertise issues, this project encountered significant delays.

We have diverted our research efforts to develop technology platform to study metastatic prostate cancer. We are able to gain fruitful outcome in 2 aspects, 1) develop cell imaging technology to assess functional activities of extracellular vesicles (EVs), and 2) develop an efficient animal system, namely the chick chorioallantoic membrane (CAM) model, to propagate advanced and metastatic prostate cancer patient-derived xenografts (PDXs).

Body

Specific Aim 1: To generate two novel PSA- and a PSMA-driven fluorescent reporter Ads and assess the dual AR functional reporter capability in prostate tumor cell lines and tumor cell spiked blood samples.

Subtask 1- Construct the AdPSA-TSTA-GFP/CMV-RFP and AdPSMA-TSTA-GFP/CMV-RFP reporter Ad.

- We have generated the 2 viral vectors. However, the functional activities of these vectors cannot be demonstrated.

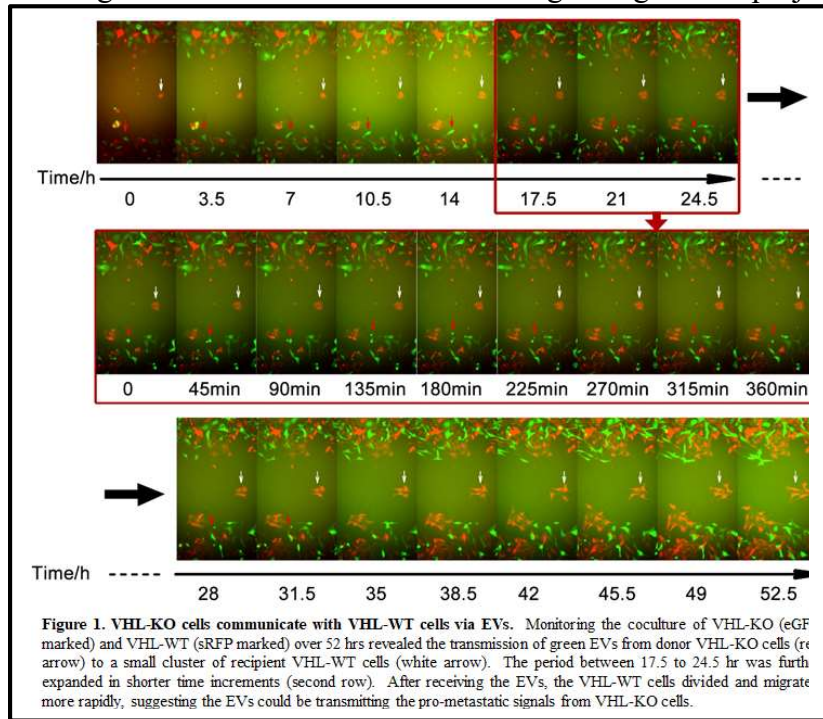
Specific Aim 2: To evaluate the functional capability of Ad-mediated CTC detection and the response to AR antagonists in the CTCs by the dual AR reporter in blood samples of CRPC patients.

- Unable to pursue this aim due to failure to generate functioning vectors.

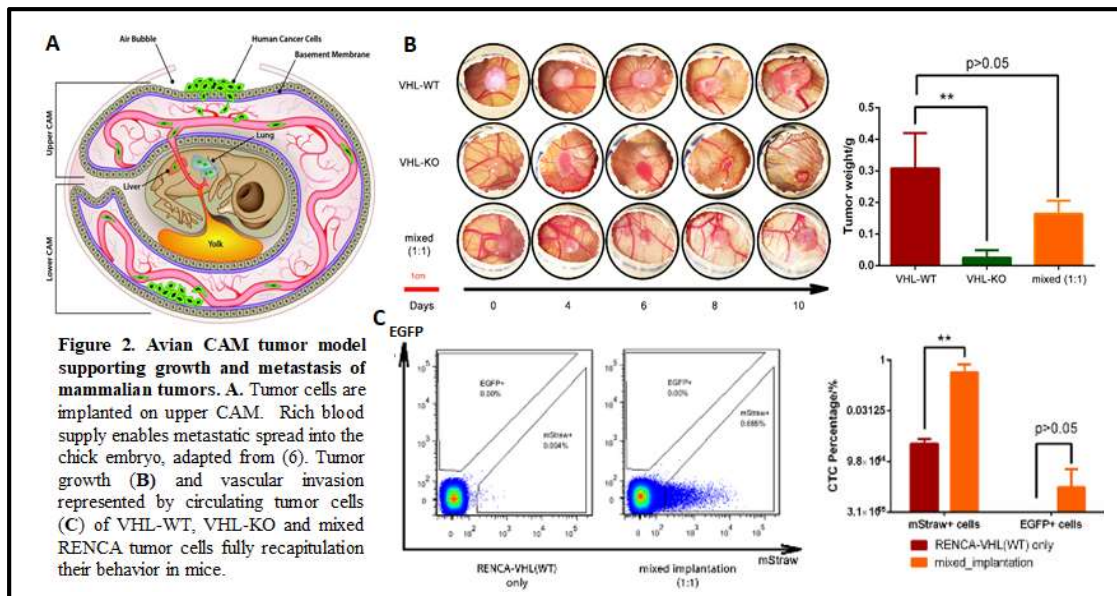
Revised Specific Aim 3: Assess extracellular vesicles (EV) in blood samples of CRPC patients. We are continuing to work with Co-I Dr. Hsian-Rong Tseng on this project

to assess the level of extracellular vesicles (EVs) produced by different prostate tumor cells. We have developed time-lapse microscopic imaging analyses to monitor the production of EVs (**Figure 1**). These cell imaging assays can complement the nanovilli microfluidic chip developed by Dr. Tseng's group in detecting EVs (3).

This enhanced metastatic activity is due to a diffusible effect that the VHL-KO cells confer on the VHL-WT, parental RENCA cells (**Figure 1**). We continue to characterize EVs in prostate cancer tumor cell lines and patient samples obtained from surgical samples. We postulate that prostate cancer also produces paracrine pro-metastatic influences. We are preparing a manuscript to describe this line of investigation.



The investigation of metastatic behaviors of prostate tumors, especially in the clinical setting, is very challenging due to the long time it takes for metastasis to develop and the



difficulty in procuring the metastatic tissues from living patients. Scientists and researchers turn to propagating patient-derived tumor tissues in immunodeficient mice to study the advanced prostate cancer. However, the tumor take rate of these patient-derived xenografts (PDXs) are rather low around 50% and the time of engraftment takes 3 months or longer. Further, the metastatic behaviors of the human disease is rarely recapitulated in mice (4). To better study prostate cancer, we took on the challenge to develop PDXs from advanced stage prostate cancer from surgical specimen using a new method of propagating, namely the chick chorioallantoic membrane (CAM) model

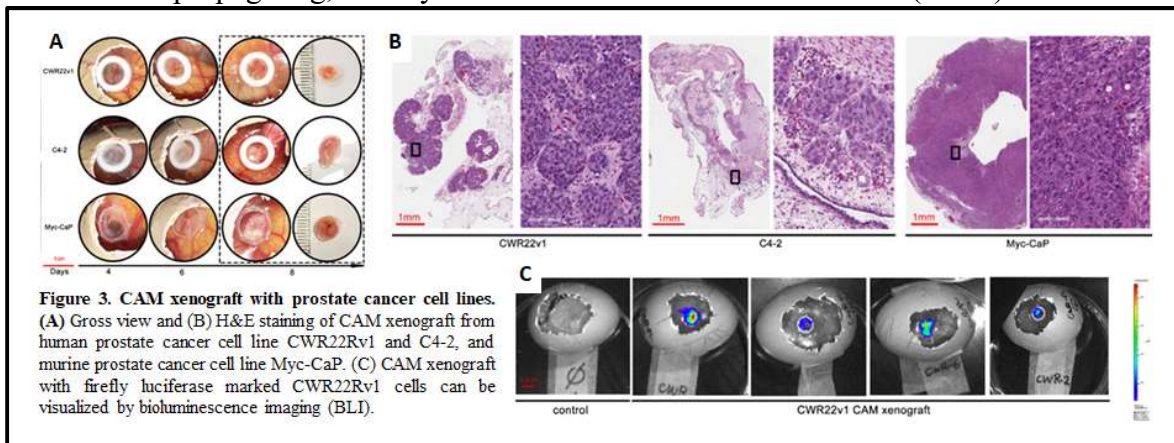
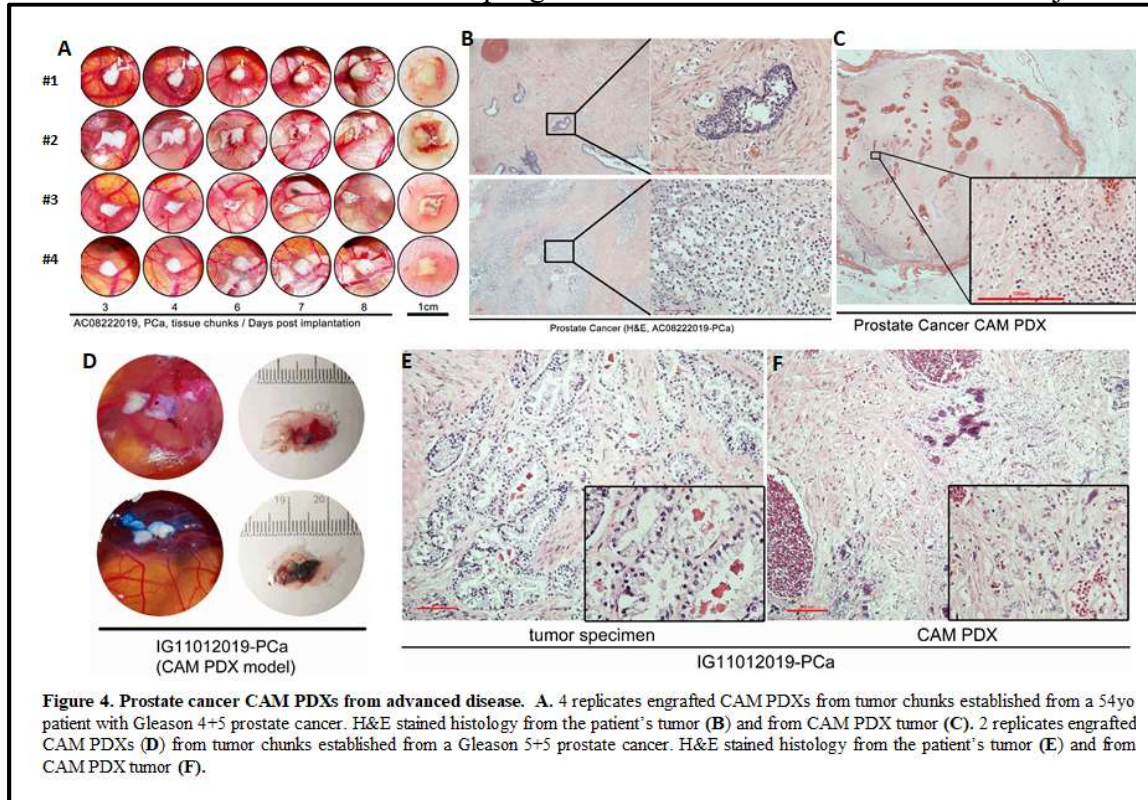


(**Figure 2A**). The CAM model has been widely used to study tumor biology for over 30 years (5). Its usage as a platform to establish PDXs is more common in the last 5-10 years. We have successfully used CAM models to establish PDXs of urological cancers such as kidney, bladder and prostate cancer in the past 3 years (7-9). More importantly, the CAM model was able to recapitulate the tumor growth and metastatic behavior of our metastatic VHL-KO RENCA RCC model (**Figure 2B, C**, 8, 9). Comparing to the mouse PDX model, the CAM PDX system has many advantages. For instance, CAM PDXs require only 10 days to establish and the growth of the PDXs can be visualized directly (**Figure 2, 3 and 4**). The cost of 1 fertilized egg is approximately \$2 in contrast to 100-fold higher cost for each immunocompromised mouse. Collectively, CAM PDXs can be established at a great saving in time, cost and labor comparing to mouse model. In our experience the CAM model efficiently supported the growth of xenografts established with all prostate cancer cell line tested, CWR22Rv1, C4-2 and MycCaP (7, **Figure 3**). Although our experience thus far on engrafting prostate cancer PDXs on CAM is limited, the take rate is 100% with 3 cases of high Gleason grade prostate cancer. The CAM model results of two representative cases are shown in **Figure 4**. We are actively investigating whether the CAM model can support the metastatic spread of human prostate cancer tumor models. Under this line of investigation, we are collaborating with Dr. Michael Freeman of Cedars Sinai Medical Center on using CAM model to investigate metastasis in NEPC.

In a related study, we investigated novel treatment approaches for CRPC patients. Docetaxel chemotherapy is often given to patients who failed ADT. We showed that inhibition of tumor associated macrophages with CSF1R kinase inhibition in conjunction



of ADT plus docetaxel significantly improved the durability of this treatment. This manuscript entitled: Inhibition of TAMs improves the response to docetaxel in castration-resistant prostate cancer, is published in Endocrine Related Cancer. The manuscript was enclosed in the last progress report. The print version is enclosed here.

Key Research Accomplishments

- We have improved exosome (EVs) purification and functional characterization methods in collaboration with Dr. Tseng's laboratory. This work has been submitted for publication. (JT Dong, RY Zhang, N Sun, J. Hu, M. Smalley, AQ Zhou, Y. Hua, W. Rothermich, A. Chen, JL Ye, PC Teng, DP Qi, MY Li, L Wu, MP Zhao, HR Tseng, YZ Zhu, Coupling Nanostructured Microchips with Covalent Chemistry Enables Purification of Sarcoma-Derived Extracellular Vesicles for Downstream Functional Studies, ACS Nano, under review)
- A paper on improved therapeutic management of CRPC has been published in Endocrine Related Cancer.
- We have refined the methodology of CAM tumor model to propagate advanced and metastatic prostate cancer. We are exploiting the efficiencies of CAM PDX model to study NEPC in collaboration with Dr. Michael Freeman. Specifically, we will assist Dr. Chen Qian, a postdoctoral fellow of Dr. Freeman, to study

NEPC. Dr. Qian was recently awarded an AUA Research Scholar fellowship entitled “Targeting ONECUT2: Differential routes to metastasis in mCRPC” with our assistance in the CAM model. Our group has published two papers describing the methodology of establishment of CAM PDXs. See Hu et al and Sharrow et al listed below. Hu et al paper is enclosed.

Reportable Outcomes

Guan W, Hu J, Yang L, Tan P, Tang Z, West B, Bollag G, Xu H, Wu L. Inhibition of TAMs improves the response to docetaxel in castration-resistant prostate cancer. *Endocrine Related Cancer*, 2019 Jan 1;26(1):131-140. doi: 10.1530/ERC-18-0284. PMID: 30400004.

Hu J, Ishihara M, Chin AI, Wu L. Establishment of xenografts of urological cancers on chicken chorioallantoic membrane (CAM) to study metastasis. *Precis Clin Med*. 2019 Sep;2(3):140-151. doi: 10.1093/pcmedi/pbz018. Epub 2019 Oct 1. PMID: 31598385

Sharrow AC, Ishihara M, Hu J, Kim IH, Wu L. Using the Chicken Chorioallantoic Membrane In Vivo Model to Study Gynecological and Urological Cancers. *J Vis Exp*. 2020 Jan 28;(155). doi: 10.3791/60651. PMID: 32065133

Conclusion

Knowledge are becoming crystallized in that CTCs isolated from the blood stream of patients with advanced metastatic castrate resistant prostate cancer (CRPC) can reflect the tumor biology of the primary tumor or disseminated disease. The original intent of this project was to advance CTC diagnostic method to improve the specificity for detecting prostate cancer CTCs. Unfortunately, due to changes in personnel in the PI’s lab, the implementation of the molecular vector construction work was unsuccessful. However, we have diverted our research efforts to develop technologies that will enhance the study of advanced and metastatic prostate cancer. Metastatic prostate cancer is the lethal stage of this disease that remains poorly understood and without an effective treatment. We have made progress in two fronts to advance in the understanding of metastatic prostate cancer. First, we have improved the ability to characterize the functional capabilities of EVs produced by advanced, aggressive cancer cells. This work is accomplished in collaboration with co-PI Dr. Tseng. Second, we have developed a new tumor model, the CAM system, to establish new prostate cancer PDXs. We are actively employing this CAM model to study NEPC in collaboration with Dr. Michael Freeman. Collectively, our research efforts supported by this DOD grant will enable a better detection and investigation of clinical-relevant, metastatic CRPC.

References

1. Diamond E, Lee GY, Akhta NH, Kirby BJ, Giannakakou P, Tagawa ST, Nanus DM. Isolation and characterization of circulating tumor cells in prostate cancer. *Front Oncol*, 2012 2:131.
2. Doyen J, Alix-Panabières C, Hofman P, Parks SK, Chamorey E, Naman H, et al. Circulating tumor cells in prostate cancer: a potential surrogate marker of survival. *Crit Rev Oncol Hematol* 2011 81: 241– 56.
3. Dong J, Zhang RY, Sun N, Smalley M, Wu Z, Zhou A, Chou SJ, Jan YJ, Yang P, Bao L, Qi D, Tang X, Tseng P, Hua Y, Xu D, Kao R, Meng M, Zheng X, Liu Y, Vagner T, Chai X, Zhou D, Li M, Chiou SH, Zheng G, Di Vizio D, Agopian VG, Posadas E, Jonas SJ, Ju SP, Weiss PS, Zhao M, Tseng HR, Zhu Y. Bio-Inspired NanoVilli Chips for Enhanced Capture of Tumor-Derived Extracellular Vesicles: Toward Non-Invasive Detection of Gene Alterations in Non-Small Cell Lung Cancer. *ACS Appl Mater Interfaces*. 2019 Apr 17;11(15):13973-13983. doi: 10.1021/acsami.9b01406. Epub 2019 Apr 2. PMID: 30892008
4. Davies, A. H., Wang, Y. & Zoubeidi, A. Patient-derived xenografts: A platform for accelerating translational research in prostate cancer. *Mol. Cell. Endocrinol* (2017).
5. Ribatti D. The chick embryo chorioallantoic membrane as a model for tumor biology. *Exp Cell Res*. Nov 1;328(2):314-24. (2014) PMID: 24972385
6. Liu M, Scanlon CS, Banerjee R, Russo N, Inglehart RC, Willis AL, Weiss SJ, D'Silva NJ. The Histone Methyltransferase EZH2 Mediates Tumor Progression on the Chick Chorioallantoic Membrane Assay, a Novel Model of Head and Neck Squamous Cell Carcinoma. *Transl Oncol*. 2013 Jun 1;6(3):273-81. PMCID: PMC3660795
25. Hu J, Ishihara M, Chin AI, Wu L. Establishment of Xenografts of Urological Cancers on Chicken Chorioallantoic Membrane (CAM) to Study Metastasis. *Precision Clinical Medicine*, 2019 Oct 1; 2(3): 140–151.
8. Ishihara M, Hu J, Wong A, Cano-Ruiz C, and Wu L. Mouse- and Patient-Derived CAM Xenografts for Studying Metastatic Renal Cell Carcinoma. In: Tamanoi F, ed. *The Enzymes: Chick Chorioallantoic Membrane Model and Precision Cancer Therapy*. Cambridge, MA: Academic Press; 2019;46:59-80.
9. Sharrow AC, Ishihara M, Hu J, Kim IH, Wu L. Using the Chicken Chorioallantoic Membrane In Vivo Model to Study Gynecological and Urological Cancers. *J Vis Exp*. 2020 Jan 28;(155). doi: 10.3791/60651. PMID: 32065133

Appendices

Guan et al. Inhibition of TAMs improves the response to docetaxel in castration-resistant prostate cancer. *Endocrine Related Cancer*, 2019 Jan 1;26(1):131-140.

Hu et al. Establishment of xenografts of urological cancers on chicken chorioallantoic membrane (CAM) to study metastasis. *Precis Clin Med*. 2019 Sep;2(3):140-151.

Supporting Data

Relevant data inserted into the body section.

RESEARCH

Inhibition of TAMs improves the response to docetaxel in castration-resistant prostate cancer

Wei Guan^{1,*}, Junhui Hu^{1,2,3,*}, Lu Yang⁴, Ping Tan⁴, Zhuang Tang⁴, Brian L West⁵, Gideon Bollag⁵, Hua Xu¹ and Lily Wu^{3,6,7,8,9}

¹Department of Urology and Institute of Urology, Tongji Hospital, Tongji Medical College, Huazhong University of Science and Technology, Wuhan, China

²Department of Paediatric Surgery, Tongji Hospital, Tongji Medical College, Huazhong University of Science and Technology, Wuhan, China

³Department of Molecular and Medical Pharmacology, David Geffen School of Medicine, University of California at Los Angeles, Los Angeles, California, USA

⁴Department of Urology, Institute of Urology, West China Hospital of Sichuan University, Chengdu, China

⁵Plexxikon Inc., Berkeley, California, USA

⁶Department of Urology, David Geffen School of Medicine, University of California at Los Angeles, Los Angeles, California, USA

⁷Department of Pediatrics, David Geffen School of Medicine, University of California at Los Angeles, Los Angeles, California, USA

⁸Jonsson Comprehensive Cancer Center, David Geffen School of Medicine, University of California at Los Angeles, Los Angeles, California, USA

⁹Molecular Biology Institute, University of California at Los Angeles, Los Angeles, California, USA

Correspondence should be addressed to L Wu: lwu@mednet.ucla.edu

*(W Guan and J Hu contributed equally to this work)

Abstract

For men with castration-resistant prostate cancer (CRPC), androgen-deprivation therapy (ADT) often becomes ineffective requiring the addition of docetaxel, a proven effective chemotherapy option. Tumor-associated macrophages (TAMs) are known to provide protumorigenic influences that contribute to treatment failure. In this study, we examined the contribution of TAMs to docetaxel treatment. An increased infiltration of macrophages in CRPC tumors was observed after treatment with docetaxel. Prostate cancer cells treated with docetaxel released more macrophage colony-stimulating factor (M-CSF-1 or CSF-1), IL-10 and other factors, which can recruit and modulate circulating monocytes to promote their protumorigenic functions. Inhibition of CSF-1 receptor kinase signaling with a small molecule antagonist (PLX3397) in CRPC models significantly reduces the infiltration of TAMs and their influences. As such, the addition of PLX3397 to docetaxel treatment resulted in a more durable tumor growth suppression than docetaxel alone. This study reveals a rational strategy to abrogate the influences of TAMs and extend the treatment response to docetaxel in CRPC.

Key Words

- ▶ CRPC
- ▶ TAMs
- ▶ docetaxel
- ▶ CSF-1
- ▶ CSF-1R

Endocrine-Related Cancer
(2019) **26**, 131–140

Introduction

Prostate cancer (PCa) is the second most common cancer in men after skin cancer, as one out of seven men will be diagnosed with this disease in the United States by 2017 (Siegel *et al.* 2017). It is estimated that 161,000 newly diagnosed cases and 27,000 deaths will be attributed to

this disease in 2017 (Siegel *et al.* 2017). A great majority of PCa patients, 70–80%, present with localized, organ-confined disease and their outcome is very favorable, having 10-year survival rate above 95%. However, 20–30% of patients will present with characteristics of high risk,

advanced disease such as high Gleason grade or distant metastases. In these cases, the 5-year survival rate drops precipitously to about 30% (Siegel *et al.* 2017).

For PCa patients with advanced disease, androgen-deprivation therapy (ADT) is the first line of treatment, developed by Dr Huggins more than 75 years ago to deplete androgen, a key growth factor for prostate cancer cells (Esch *et al.* 2014). Over the years, effective strategies of ADT include the depletion of the body's source of androgen by inhibiting androgen biosynthesis pathways and by blocking the activation of androgen receptor (AR) (Merseburger *et al.* 2015). Abiraterone and enzalutamide are two newly approved potent ADT agents that inhibit CYP17A1 androgen synthetic enzyme and AR, respectively (de Bono *et al.* 2011, Scher *et al.* 2012). Both agents are effective in prolonging the survival of castration-resistant prostate cancer (CRPC) patients who had progressed on first-line ADT (Ryan *et al.* 2015). However, a significant proportion of CRPC patients either do not respond to either abiraterone or enzalutamide, or initially respond but subsequently progress on treatment (Silberstein *et al.* 2016). Potential mechanisms of resistance include AR mutations, amplification and splice variant (Antonarakis *et al.* 2014, Azad *et al.* 2015, Romanel *et al.* 2015).

Docetaxel has been established as the standard first-line chemotherapy agent to treat CRPC since 2004. It was approved by FDA for this purpose as several large clinical trials showed docetaxel containing regimens provided survival benefits over other chemotherapies for CRPC patients (Petrylak *et al.* 2004, Tannock *et al.* 2004, Sweeney *et al.* 2015). Belonging to the taxane family, docetaxel was initially postulated to suppress prostate cancer growth by interfering with microtubule function (Petrylak 2003). However, subsequent research supported that the therapeutic activity of taxanes in prostate cancer could arise from its interference with androgen signaling via the nuclear translocation process (Gan *et al.* 2009).

Given taxane-based chemotherapy is one of a few effective treatments for CRPC, we investigate a rational combination regimen to improve its therapeutic efficacy. Recent findings from our group and others showed that tumor-associated macrophages (TAMs) contribute significantly to treatment failure in PCa and other solid cancers via their wound-healing and protumorigenic functions (Xu *et al.* 2013, Escamilla *et al.* 2015, Brown *et al.* 2017). In this study, we employed a small-molecule CSF1R kinase inhibitor (CSF-1Ri), PLX3397, to block TAMs in CRPC models. In combination with ADT and docetaxel, PLX3397 was able to significantly reduce the number of infiltrating TAMs and lower their protumorigenic

influences. We showed that the addition of PLX3397 extended the therapeutic response to ADT and docetaxel in CRPC models.

Materials and methods

Cell culture and drugs

The murine macrophage RAW264.7 (RAW) cells (ATCC) and MyC-CaP cells (a kind gift from Dr. Charles Sawyers, Memorial Sloan Kettering New York) were cultured with DMEM (high glucose) while PC3 (ATCC), CWR22Rv2 (a kind gift from Dr. David Agus, Cedars-Sinai Medical Center) and LNCap-C4-2 (C4-2) cells (ATCC) were cultured in RPMI-1640. Both media were supplemented with 10% fetal bovine serum (FBS), 100U/mL penicillin and 100µg/mL streptomycin. PLX3397, 5-[[5-chloro-1H-pyrrolo[2,3-b]pyridin-3-yl)methyl]-N-[[6-(trifluoromethyl)-3-pyridyl]methyl]pyridin-2-amine was synthesized at Plexikon Inc. The detailed synthetic procedure is shown by Tap *et al.* (2015).

Transwell coculture and migration assay

In coculture assay, 1.0×10^6 RAW macrophages were seeded in transwell inserts with membrane pore size at 4µm (BD Falcon) in media supplemented with 2µM PLX3397, 1µM GW2580 or DMSO vehicle. The chamber was inserted in a 6-well plate with conditioned media from Myc-CaP, PC3, CWR and C4-2 cells treated with docetaxel (100nM for MyC-CaP, 5nM for CWR22Rv1, 30nM for PC3 and 2nM for C4-2 cells) or DMSO. Total RNA was extracted from tumor cells after 48h and analyzed by RT-PCR. The methods for RT-PCR is described in Supplementary data (see section on [supplementary data](#) given at the end of this article) and primers are listed in Supplementary Table 1.

In migration assay, 1.0×10^5 RAW cells were seeded in transwell inserts with membrane pore size at 8µm assembled in 24-well plates. The number of migrated cells was evaluated after 6h of incubation at 37°C, and then treated with 3% paraformaldehyde (PFA) and stained with 0.1% (w/v) crystal violet solution. Random 10 fields/well at 4× magnification were sampled and quantified with ImageJ2.

ELISA assay

1.0×10^6 MyC-CaP, PC3, CWR and C4-2 cells were cocultured with or without RAW cells as mentioned earlier, with or without Docetaxel or PLX3397 at tumor cells' IC₅₀ or IC₁₀ concentrations.

Supernatant of all cell culture media were harvested after 48 h. 96-well Nunc MaxiSorp Plates (Cat#44-2404-21, Thermo Scientific) were coated with the anti-M-CSF antibody (1:300, Cat#sc-365779, Santa Cruz Biotech) in coating buffer diluted from Coating Solution Concentrate Kit (KPL) at 4°C overnight. Then, the plate was washed with 1× wash buffer (KPL) and blocked with 1% BSA Blocking Solution (KPL) for 1 h at room temperature. Cell supernatant was added to the wells and incubated for 1 h at room temperature in the shaker at 220 rpm. After washing with 1× wash buffer (KPL), each well was incubated with the second anti-M-CSF antibody (1:300, Cat#sc-13103, Santa Cruz Biotech) overnight at 4°C. The wells were washed four times, 5 min for each and incubated with 100 µL of HRP-conjugated goat-anti-rabbit IgG (1:5000, Cat# 111-035-045, Jackson Laboratory) for 1 h at room temperature. The wells were washed four times, 5 min for each and incubated with 100 µL of ABTS ELISA HRP Substrate (KPL). Absorbance at 410 nm was measured by Synergy HT microplate reader (BioTek).

Flow cytometry

MyC-CaP cells were cocultured with or without RAW cells, docetaxel (IC₁₀ or IC₅₀) for 48 h before cells were trypsinized. Single cell suspension was rinsed with PBS twice and incubated with APC conjugated anti-IL-10 antibody (Cat#17-7101-82, eBioscience) for 30 min at 4°C at darkness. Cell acquisition was done on a BD LSR-II flow cytometer (Beckman Coulter) and data were analyzed by FlowJo software (TreeStar).

For tumor tissue analysis, single cell suspension was prepared by digestion of collagenase II at 0.1% for 1 h. Then, cells were counted and incubated with APC-conjugated anti-CD11b antibody (Cat#17-0112-81, eBioscience) and PE-conjugated anti-CSF1R antibody (Cat#12-1152-82, eBioscience) for 30 min at 4°C in darkness.

MyC-CaP subcutaneous xenograft model

All animal experiments were approved by the Animal Research Committee of the University of California, Los Angeles. For MyC-CaP s.c. xenograft model, 16 FVB male mice that are 6–8 weeks old from Taconic Biosciences were adopted and kept at BSL2 animal facility. After trypsinization and rinsing with cooled PBS, 1.0×10⁶ MyC-CaP cells were resuspended in 200 µL PBS/Matrigel (1:2) (356230, Corning) and injected with insulin syringe into the subcutaneous space on the right back of FVB male mice (*n*=16). One week after the cell injection,

mice were castrated and divided randomly into four groups, receiving DMSO vehicle+control chow, DMSO vehicle+chow containing PLX3397, docetaxel+control chow or docetaxel+chow containing PLX3397. The PLX3397 dosage is 40 mg/kg/day on average and docetaxel dosage is 40 mg/kg/week. Tumor size was measured by digital calipers and calculated by the formula $V=0.5*a*b^2$, in which *a* is the larger and *b* is the smaller index of the two perpendicular indexes of the tumor.

CWR22Rv1 orthotopic xenograft model

After trypsinization and rinsing with precooled PBS, 1×10⁵ CWR22Rv1 cells, stably expressing firefly luciferase, were resuspended in 10 µL of PBS/Matrigel (1:2) (356230, Corning) and injected by insulin syringe into the left anterior lobe of prostate gland of 6–8 weeks old SCID-beige male mice (Jackson Laboratory). All mice were castrated on day 14 post injection and randomly divided into two groups, receive docetaxel+control chow or docetaxel+PLX3397 chow (40 mg/kg/day). The docetaxel treatment started on day 19 at 10 mg/kg/week. The *in vivo* BLI were performed every week and the luminescence count was recorded as previously described (Palmeri *et al.* 2008). All mice were killed on day 42.

Statistical analysis

Data are all presented as mean±s.e.m. Student *t*-test was used for comparison between two groups while two-way ANOVA was used for comparisons between multiple groups.

Results

Docetaxel-mediated tumor cell injury induces the expression of M2 cytokines

To study the impact of docetaxel in prostate cancer, we first examined the dose response of this chemotherapeutic agent on several prostate cancer cell lines (Fig. 1A). We found that PCa cells exhibit a wide range of sensitivity to docetaxel, with C4-2 (IC₅₀=2 nM) and CWR22Rv1 (IC₅₀=5 nM) being the most sensitive, PC-3 (IC₅₀=30 nM) as an intermediate responder and MyC-CaP (IC₅₀=100 nM) being the most resistant. As we have shown in previous studies, conventional cytotoxic therapies such as radiation therapy and ADT all can induce PCa cells to express M2 cytokines (Xu *et al.* 2013, Escamilla *et al.* 2015). Here, we further inquired whether docetaxel in addition to

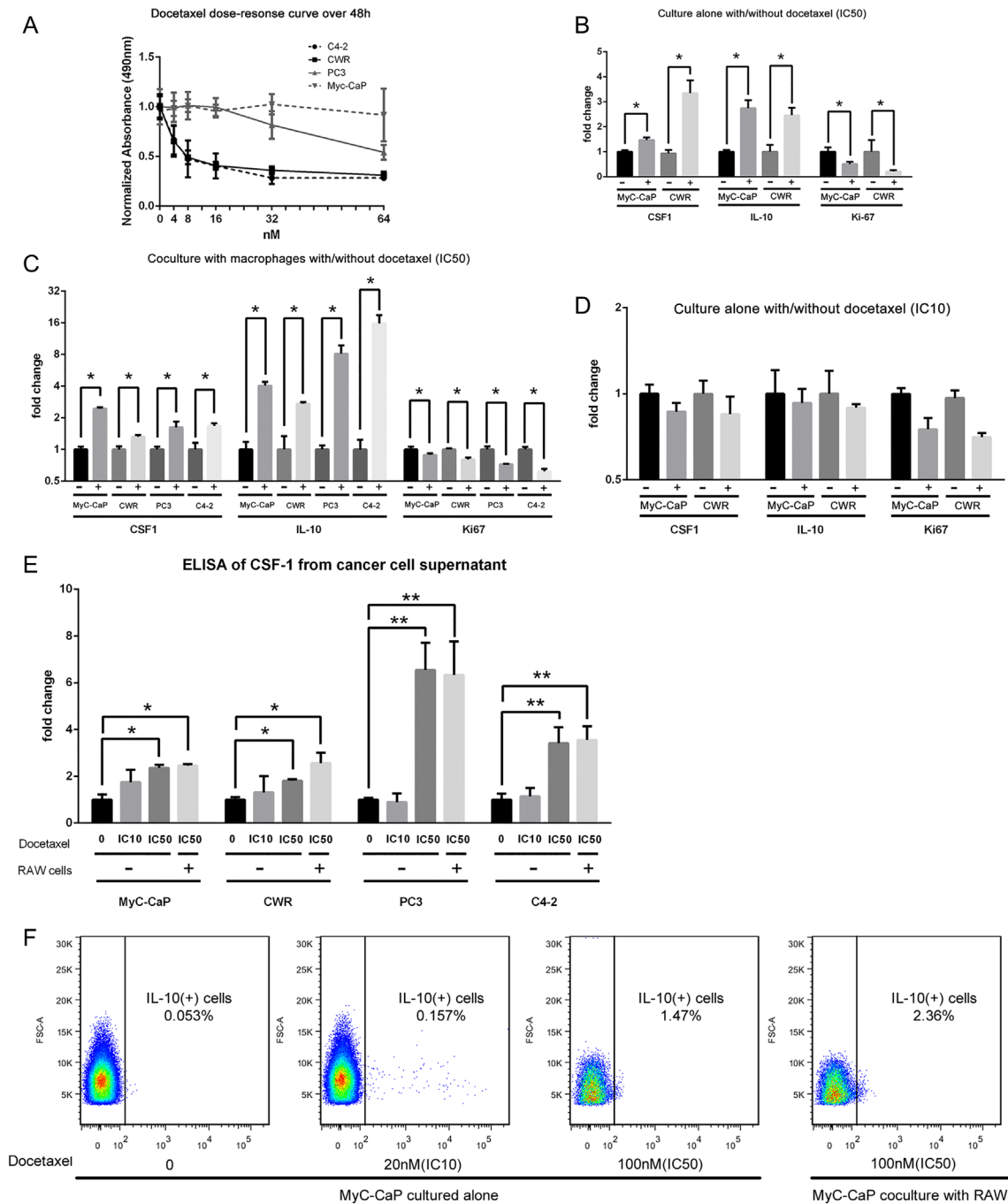


Figure 1

Cytokine expression upon docetaxel treatment in prostate cancer cells. (A) The dose–response curve was plotted in different working concentrations of docetaxel for C4-2, CWR22Rv1, PC3, MyC-CaP cells to determine their respective IC₅₀ and IC₁₀ values. (B) MyC-CaP and CWR22Rv1 cells, cultured alone were treated with docetaxel at the IC₅₀ dose for each cell (Myc-CaP at 100 nM and CWR22Rv1 at 5 nM). Expression of CSF-1 and IL-10 and Ki-67 in response to docetaxel treatment was shown. (C) The impacts of docetaxel treatment at IC₅₀ on Pca cells in the presence of macrophages (RAW cells) were shown for MyC-CaP, CWR22Rv1, PC3 (30 nM) and C4-2 (2 nM) cells were shown (D). When treated at their respective IC₁₀ doses of 20 and 1 nM, MyC-CaP and CWR22Rv1 cells showed no significant change in CSF-1, IL-10 or Ki67 expression. (E) The level of secreted CSF-1 in culture supernatant from MyC-CaP, CWR22Rv1, PC3 and C4-2 cells treated with docetaxel at IC₁₀ or IC₅₀, and with and without co-cultured with RAW macrophages, were analyzed by ELISA. (F) Intracellular IL-10 expression in MyC-CaP cells treated with docetaxel at IC₁₀ or IC₅₀, with and without co-cultured with RAW macrophages, were analyzed by flow cytometry. All cells were cultured in media supplemented with charcoal-stripped serum (**P* < 0.05, ***P* < 0.01).

ADT would also induce the expression of M2 cytokines such as CSF-1 and IL-10. To mimic ADT, all prostate cancer cells were cultured in media supplemented with charcoal-treated fetal bovine serum (FBS) to remove the androgens. As shown in Fig. 1B MyC-CaP or CWR22Rv1 cells treated with ADT plus docetaxel, dosed at each line's respective IC_{50} , increased the expression of CSF-1 and IL-10. Likewise, the expression of these M2 cytokines was also induced when PCa cells, including MyC-CaP, CWR22Rv1, PC3 and C4-2, were treated in the presence of macrophages (Fig. 1C). This ADT plus docetaxel treatment resulted in a significant reduction in cell proliferation, as indicated by the decrease in the proliferative marker Ki67. Interestingly, when the PCa cells were treated with a lower dose of docetaxel at the IC_{10} dose, the elevation of M2 cytokine expression was no longer observed (Fig. 1D). Docetaxel treatment induced increase in CSF-1 and IL-10 in the tumor cells were further analyzed and verified at the protein level by CSF-1 ELISA (Fig. 1E) and IL-10 flow cytometry (Fig. 1F). This induction of M2 cytokines is likely not restricted to docetaxel alone. We observed very

similar effects with paclitaxel treatment of all four PCa cell lines (Supplementary Fig. 1). Collectively, these findings support that cell injury mediated by ADT plus docetaxel induces the heightened expression of M2 cytokines in PCa cells.

Docetaxel induces CSF-1 expression and increases the recruitment of macrophages *in vitro*

CSF-1 or M-CSF is a cytokine critical not only in the differentiation and proliferation of myeloid cells but also in the recruitment and polarization of protumorigenic M2 macrophages (Brown *et al.* 2017). Next, we examine the impact of macrophage recruitment in the setting of docetaxel treatment. As shown in Fig. 2A and B, CWR22Rv1 and C4-2 PCa cells treated with docetaxel were able to recruit more macrophages in an *in vitro* transwell assay compared to chemo-naïve cells. The elevated CSF-1 produced by the docetaxel-treated PCa cells likely contributed to the increased macrophage recruitment, as the addition of the CSF-1Ri PLX3397 attenuated the

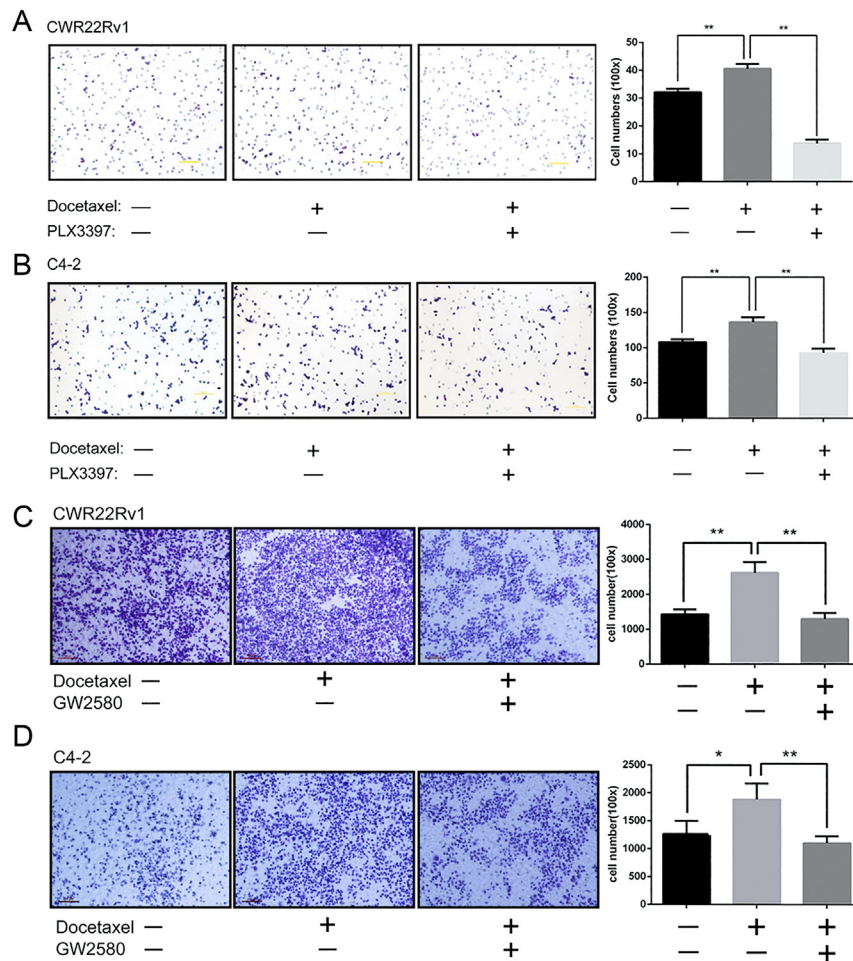


Figure 2

CSF-1R inhibitor PLX3397 abrogated the increased recruitment of macrophages induced by docetaxel treatment *in vitro*. Conditioned media of CWR22Rv1 (A) and C4-2 (B) prostate cancer cells treated with docetaxel was able to recruit more RAW macrophages migrating across a transwell porous membrane than media from untreated cells. The addition of 2 μ M CSF-1Ri PLX3397 to the docetaxel treated conditioned media abrogated the increased macrophage recruitment induced by both cell lines. In a second set of similar study, the increase in RAW macrophages migration by CWR22Rv1 (C) and C4-2 (D) conditioned media was inhibited by 1 μ M GW2580, a selective CSF-1R kinase inhibitor (* $P < 0.05$, ** $P < 0.01$).

enhancement in macrophage recruitment *in vitro* (Fig. 2A and B), as we and others have previously reported (Xu *et al.* 2013, Escamilla *et al.* 2015, Moughon *et al.* 2015, Butowski *et al.* 2016).

PLX3397 is known to also inhibit c-Kit (Tap *et al.* 2015). We employed a second highly selective CSF-1R kinase inhibitor GW2580 to substantiate that CSF1/CSF1R as the key signal axis for macrophage recruitment (Priceman *et al.* 2010). As shown in Fig. 2C and D, the enhancement of macrophage recruitment across a transwell mediated by docetaxel-treated PCa cells was dampened significantly by the addition of GW2580.

Adding CSF-1R kinase inhibitor, PLX3397, to docetaxel regimen enhances therapeutic efficacy in CRPC

Next, we investigated the impact of docetaxel treatment on macrophage recruitment *in vivo* in CRPC tumors. We first evaluated TAMs in the MyC-CaP tumors engrafted subcutaneously in syngeneic FVB male mice. One week after tumor cell implantation, tumor-bearing mice were treated with surgical castration as ADT, and divided into four treatment groups receiving (i) diluent control, (ii) oral PLX3397, (iii) docetaxel or (iv) docetaxel plus PLX3397. The PLX3397 treatment was administered orally via rodent chow and docetaxel was administered IP at 40 mg/kg/week. Comparing to diluent control-treated tumors, PLX3397 only treatment significantly reduced the number of CD11b⁺ CSF1R⁺ TAMs, while docetaxel significantly increased TAMs (Fig. 3A and B). Importantly, the addition of PLX3397 to docetaxel-treated group was able to not only reverse the chemotherapy-induced TAM influx but suppressed the TAM level in the tumor below that of the control treated group (Fig. 3A and B). These results demonstrate the importance of CSF-1/CSF-1R axis in the recruitment of macrophages and the effectiveness of PLX3397 in blocking this CSF-1R-mediated TAM recruitment *in vitro* and *in vivo*.

In our previous therapeutic studies, we consistently observed that CSF-1R blockade treatment alone can reduce the infiltration of TAMs but exert negligible impact on tumor growth *in vivo* (Priceman *et al.* 2010, Xu *et al.* 2013, Escamilla *et al.* 2015, Butowski *et al.* 2016). The same result was observed here in the MyC-CaP tumors: no significant reduction in tumor growth was observed after oral PLX3397 treatment alone despite clear reduction in the level of TAMs in the tumor (Fig. 3C, D and E). As expected, docetaxel treatment significantly retarded the growth of MyC-CaP tumor compared to control (Fig. 3C, D and E). More importantly, docetaxel plus PLX3397 achieved the

most significant tumor growth suppression in the four treatment groups, more effective than docetaxel alone (Fig. 3C, D and E).

Next, we asked whether the benefit of PLX3397 in combination with docetaxel in the subcutaneous MyC-CaP model can also be observed in the orthotopic prostatic environment of the CWR22Rv1 model. SCID/Beige male mice received intraprostatic injection of firefly luciferase-labeled CWR22Rv1 cells, such that tumor growth can be monitored in real time by bioluminescence imaging (BLI, Fig. 3F and G). On day 14 after tumor cell implantation, mice received ADT via surgical castration. On day 19, tumor-bearing mice received either docetaxel with control or docetaxel plus oral PLX3397 (Fig. 3B). Treatment continued to day 42, at which point the animals were killed. Assessed either by BLI (Fig. 3F and G) or by terminal tumor volume (Fig. 3H and I), the docetaxel plus PLX3397 group consistently showed significantly greater efficiency in suppressing tumor growth over docetaxel treatment alone. Again, corroborating our prior findings, the added oral PLX3397 drastically reduced the level of CD11b⁺ CSF1R⁺ TAMs from 10.6% in the docetaxel only group to 0.1% in the docetaxel plus PLX3397 group, as analyzed by flow cytometry (Fig. 3J). This finding was further verified by F4/80 immunohistochemistry stain to detect macrophages (Fig. 3K). The functional consequences of TAM inhibition by PLX3397 included lowering angiogenic drive, tissue remodeling and immunosuppression as assessed by VEGF-A, MMP-9 and Arg-1 expression respectively (Fig. 3F and G). Taken together, we have shown that the use of a selective CSF-1Ri PLX3397 can block the infiltration of TAMs into prostate tumor and thus reduce the protumorigenic influences of M2 macrophages by lowering tumoral angiogenesis, tissue remodeling and immunosuppression leading to more effective treatment response to docetaxel.

Discussion

Docetaxel is a widely used chemotherapeutic agent in treating breast cancer (Palmeri *et al.* 2008), head and neck cancer (Rapidis *et al.* 2008) and non-small-cell lung cancer (Fossella 2002). In the Chemohormonal Therapy vs Androgen Ablation Randomized Trial for Extensive Disease (CHAARTED) randomized phase III trial, men with hormone-naive metastatic PCa were randomly assigned to receive docetaxel plus ADT or ADT alone, with nearly 400 men in each arm. In particular, patients who had high-volume disease benefited the most with docetaxel, achieving a very significant prolongation of their median

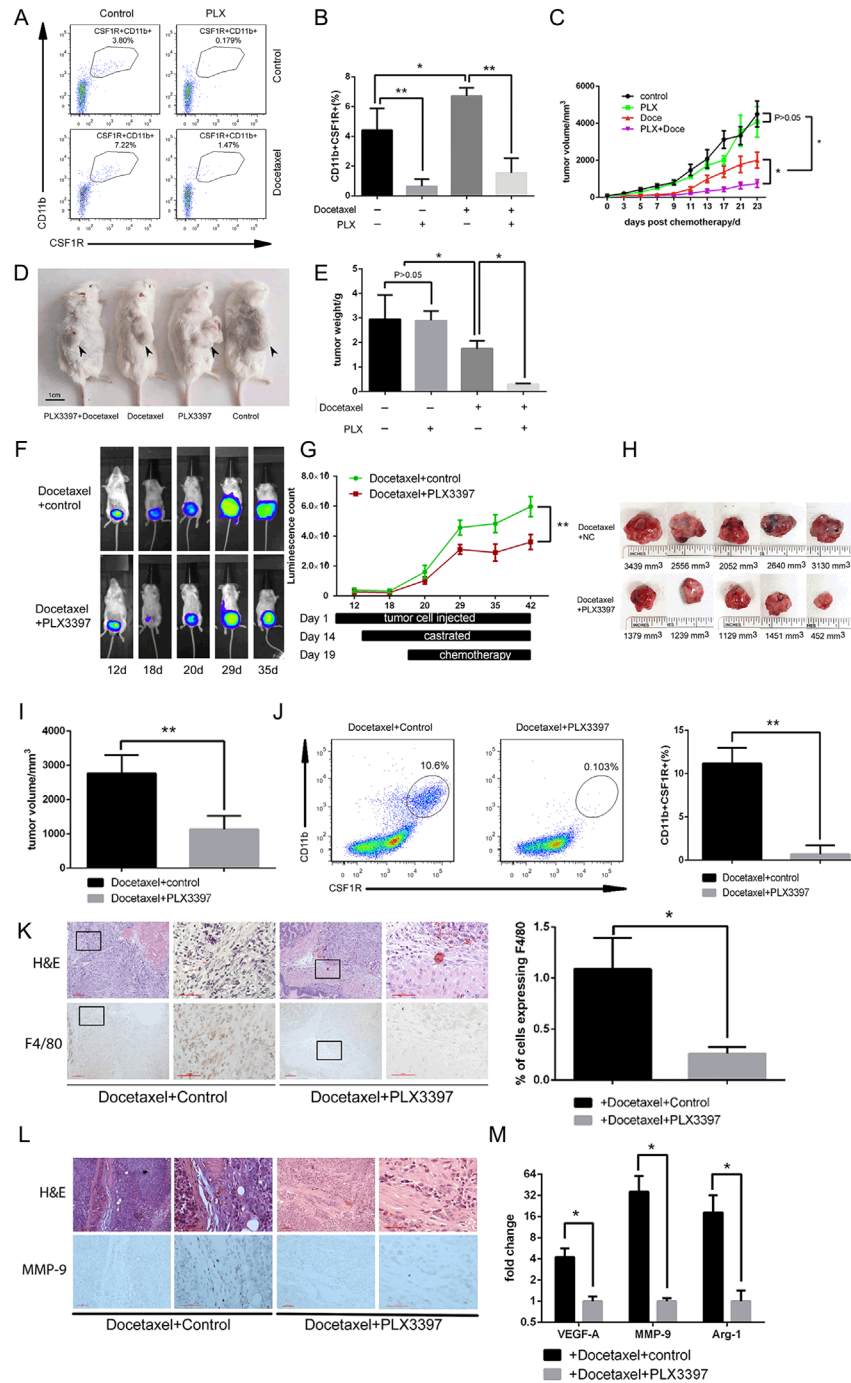


Figure 3

The addition of PLX3397 to docetaxel improves therapeutic efficacy in CRPC by reducing the protumorigenic influences of TAMs. The therapeutic effects of combining CSF-1Ri PLX3397 with docetaxel were evaluated in subcutaneous Myc-CaP tumors established in FVB male mice. Seven days after tumor cell implantation, all mice received surgical castration and randomly assigned to 4 treatment groups: (i) control, (ii) PLX3397, (iii) docetaxel or (iv) docetaxel + PLX3397. Flow cytometric analyses of CD11b+CSF1R+ TAM population in the tumor were shown as individual representative flow plots (A) and for each treatment cohort (B). Longitudinal tumor volume (C) and final tumor size (D and E) were shown for the four treatment groups. Intraprostatic CWR22Rv1 tumors were established with firefly luciferase marked cells, and longitudinal tumor growth were monitored by *in vivo* BLI (F and G). Tumor growth suppression was more effective in the docetaxel + PLX3397 group compared to the docetaxel only group (H and I) as assessed by terminal tumor volume. Likewise the PLX3397 containing treatment group was significantly reduced in the proportion of CD11b+ CSF1R+ TAM as analyzed by flow cytometry (J), and immunohistochemistry with F4/80 macrophages (K) and the tissue remodeling marker MMP-9 (L). Gene expression profiling by qRT-PCR revealed a reduction in VEGF-A, MMP-9 and Arg-1 with CSF-1Ri treatment (M) (* $P < 0.05$, ** $P < 0.01$).

survival by 17 months compared to ADT alone (Azad *et al.* 2015). Hence, docetaxel is an important therapeutic agent in the armamentarium against CRPC.

In this study, we investigated whether TAMs, an important component of the tumor microenvironment, could influence CRPC's response to docetaxel. We postulate that cellular damage sustained during docetaxel treatment induces PCa cells to produce cytokines and chemokines that recruit and polarize macrophages to the protumorigenic, alternatively activated M2 subtype (Brown *et al.* 2017). Congruent with this concept, we observed a significant increase in the expression of M2 cytokines, such as CSF-1 and IL-10 in all four prostate cancer cell lines, MyC-CaP, PC-3, CWR22Rv1 and C4-2, after docetaxel treatment. The elevated CSF-1 led to increased infiltration of macrophages *in vitro* and TAMs in MyC-CaP and CWR22Rv1 tumors after ADT and docetaxel treatment. We observed that treatment with another chemotherapeutic agent, paclitaxel, also elicited an increase in M2 cytokine expression in PCa, parallel the findings of a comprehensive chemotherapeutic study in preclinical breast cancer (DeNardo *et al.* 2011). Importantly, these findings support the rational combination of CSF-1Ri with docetaxel to lower the recruitment and M2 polarization of TAMs, which in turn reduce the protumorigenic influences of TAMs and significantly increase the efficacy of tumor growth suppression of ADT and docetaxel treatment (Fig. 4).

As the emergence of resistance to the current therapies is expected, what new and effective therapies will be incorporated to treat CRPC? A second-line taxane, cabazitaxel, was developed to overcome this resistance problem. The effectiveness of docetaxel is limited by its affinity for P-glycoprotein, an ATP-dependent drug efflux pump that decreases the intracellular concentrations of drugs (Bradshaw & Arceci 1998). Cabazitaxel exhibits low affinity for P-glycoprotein and has been shown to be effective in docetaxel-refractory PCa patients (de Bono *et al.* 2010, Paller & Antonarakis 2011). Although the cancer vaccine Sipuleucel-T was approved for CRPC, current clinical experience suggests this therapy has limited efficacy for aggressive large volume disease (Schellhammer *et al.* 2013, Mok *et al.* 2014). New immunotherapeutic strategies for CRPC need further exploration. In this regard, TAMs could have multiple negative influences. For instance, M2 macrophages are well known to impair T-cell responses by depleting essential nutrients through arginase I or by inhibiting T-cell receptor CD3ζchain (Rodriguez *et al.* 2004, Munder *et al.* 2006). Interestingly, a recent study by Gordon *et al.* (2017) further implicated that PD-1 expressing TAMs are inhibiting tumor immunity, which might further empower the efficacy of the PD-1 or PD-L1 checkpoint blockade.

In our collective experience of studying TAM's influences in cancer therapy, we observed that TAMs

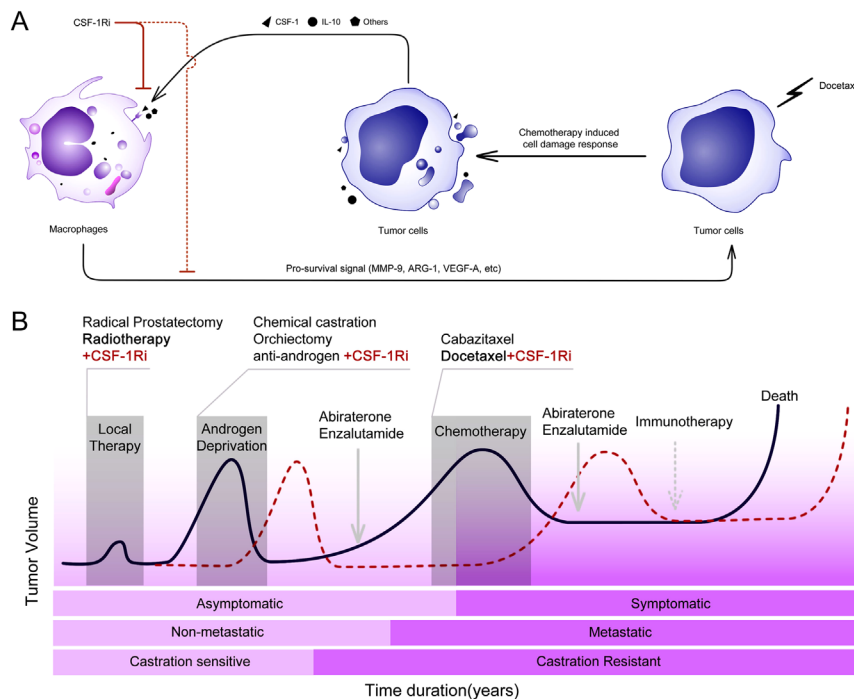


Figure 4 TAMs' contribution to docetaxel treatment failure in prostate cancer. (A) schematic illustration of impact of docetaxel treatment in PCa. The cellular damage caused by docetaxel heightens expression of M2 cytokines such as CSF-1 and IL-10, which recruit and polarize more M2 TAMs to foster their protumorigenic influences in the tumor microenvironment. The use of CSF-1R inhibitors could disrupt this TAM mediated vicious cycle. (B) The disease progression and treatment options of different stages of prostate cancer.

contribute to every stage of PCa progression and therapy. From the control of local disease by radiation therapy (Xu *et al.* 2013), to the implementation of ADT for more advanced disease (Escamilla *et al.* 2015), to the use of docetaxel in recurrent CRPC studied here, blocking TAMs with CSF-1Ri in conjunction with these conventional therapies consistently improved therapeutic outcome by prolonging the duration of tumor growth suppression. Of note, the use of CSF-1Ri alone has no therapeutic impact in numerous preclinical models we have studied, including PCa, melanoma and lung cancer (Priceman *et al.* 2010). A large volume of literature shows that macrophages are educated and polarized by the tumor microenvironment towards the protumorigenic M2 subtype (Brown *et al.* 2017). We deduced that in the face of cellular injuries induced by conventional therapies, tumor cells secrete a higher level of M2 cytokines and chemokines such as CSF-1, CCL2 and IL10 that accentuate the protumorigenic functions of TAMs. Thus, combining CSF-1Ri with conventional cytotoxic therapies is a rational approach to improve their effectiveness. As we have shown that CSF-1Ri can improve the efficacy of adoptive T-cell therapy (Mok *et al.* 2014), it will be prudent to consider the incorporation of TAM blockade in combination for future immunotherapy strategies developed for CRPC, be it checkpoint inhibition or CAR T-cell therapy or others (Bilusic *et al.* 2017). Given the critical role of TAMs in therapeutic setting for PCa, we envision that the incorporation of TAM blockade could extend the efficacy of all phases of treatment. In doing so, we could extend the survival of PCa patients and achieve the goal of transforming PCa into a chronic and survivable malignancy.

Supplementary data

This is linked to the online version of the paper at <https://doi.org/10.1530/ERC-18-0284>.

Declaration of interest

The authors declare that there is no conflict of interest that could be perceived as prejudicing the impartiality of the research reported.

Funding

This project was supported by the CDMRP PCRP award W81XWH12-1-0206 and W81XWH 15-1-0256 to L Wu. Flow cytometry and tissue process/immunohistochemical analyses were performed by Flow Cytometry Core Facility and Translational Pathology Core Laboratory of UCLA Jonsson Comprehensive Cancer Center, and UCLA CTSI (NIH P50CA16042 and UL1TR001881). Through a sponsored research agreement, Plexikon Co. supported this investigation by kindly providing the PLX3397.

References

- Antonarakis ES, Lu C, Wang H, Lubner B, Nakazawa M, Roeser JC, Chen Y, Mohammad TA, Chen Y, Fedor HL, *et al.* 2014 AR-V7 and resistance to enzalutamide and abiraterone in prostate cancer. *New England Journal of Medicine* **371** 1028–1038. (<https://doi.org/10.1056/NEJMoa1315815>)
- Azad AA, Volik SV, Wyatt AW, Haegert A, Le Bihan S, Bell RH, Anderson SA, McConeghy B, Shukin R, Bazov J, *et al.* 2015 Androgen receptor gene aberrations in circulating cell-free DNA: biomarkers of therapeutic resistance in castration-resistant prostate cancer. *Clin Cancer Research* **21** 2315–2324. (<https://doi.org/10.1158/1078-0432.CCR-14-2666>)
- Bilusic M, Madan RA & Gulley JL 2017 Immunotherapy of prostate cancer: facts and hopes. *Clin Cancer Research* **23** 6764–6770. (<https://doi.org/10.1158/1078-0432.CCR-17-0019>)
- Bradshaw DM & Arceci RJ 1998 Clinical relevance of transmembrane drug efflux as a mechanism of multidrug resistance. *Journal of Clinical Oncology* **16** 3674–3690. (<https://doi.org/10.1200/JCO.1998.16.11.3674>)
- Brown JM, Recht L & Strober S 2017 The promise of targeting macrophages in cancer therapy. *Clinical Cancer Research* **23** 3241–3250. (<https://doi.org/10.1158/1078-0432.CCR-16-3122>)
- Butowski N, Colman H, De Groot JF, Omuro AM, Nayak L, Wen PY, Cloughesy TF, Marimuthu A, Haidar S, Perry A, *et al.* 2016 Orally administered colony stimulating factor 1 receptor inhibitor PLX3397 in recurrent glioblastoma: an Ivy Foundation Early Phase Clinical Trials Consortium phase II study. *Neuro-Oncology* **18** 557–564. (<https://doi.org/10.1093/neuonc/nov245>)
- de Bono JS, Oudard S, Ozguroglu M, Hansen S, Machiels JP, Kocak I, Gravis G, Bodrogi I, Mackenzie MJ, Shen L, *et al.* 2010 Prednisone plus cabazitaxel or mitoxantrone for metastatic castration-resistant prostate cancer progressing after docetaxel treatment: a randomised open-label trial. *Lancet* **376** 1147–1154. ([https://doi.org/10.1016/S0140-6736\(10\)61389-X](https://doi.org/10.1016/S0140-6736(10)61389-X))
- de Bono JS, Logothetis CJ, Molina A, Fizazi K, North S, Chu L, Chi KN, Jones RJ, Goodman OBJ, Saad F, *et al.* 2011 Abiraterone and increased survival in metastatic prostate cancer. *New England Journal of Medicine* **364** 1995–2005. (<https://doi.org/10.1056/NEJMoa1014618>)
- DeNardo DG, Brennan DJ, Rexhepaj E, Ruffell B, Shiao SL, Madden SF, Gallagher WM, Wadhvani N, Keil SD, Junaid SA, *et al.* 2011 Leukocyte complexity predicts breast cancer survival and functionally regulates response to chemotherapy. *Cancer Discovery* **1** 54–67. (<https://doi.org/10.1158/2159-8274.CD-10-0028>)
- Escamilla J, Schokrpur S, Liu C, Priceman SJ, Moughon D, Jiang Z, Pouliot F, Magyar C, Sung JL, Xu J, *et al.* 2015 CSF1 receptor targeting in prostate cancer reverses macrophage-mediated resistance to androgen blockade therapy. *Cancer Research* **75** 950–962. (<https://doi.org/10.1158/0008-5472.CAN-14-0992>)
- Esch L, Schulz WA & Albers P 2014 Sequential treatment with taxanes and novel anti-androgenic compounds in castration-resistant prostate cancer. *Oncology Research and Treatment* **37** 492–498. (<https://doi.org/10.1159/000365530>)
- Fossella FV 2002 Docetaxel in second-line treatment of non-small-cell lung cancer. *Clinical Lung Cancer* **3** (Supplement 2) S23–S28. (<https://doi.org/10.3816/CLC.2002.s.010>)
- Gan L, Chen S, Wang Y, Watahiki A, Bohrer L, Sun Z, Wang Y & Huang H 2009 Inhibition of the androgen receptor as a novel mechanism of taxol chemotherapy in prostate cancer. *Cancer Research* **69** 8386–8394. (<https://doi.org/10.1158/0008-5472.CAN-09-1504>)
- Gordon SR, Maute RL, Dulken BW, Hutter G, George BM, McCracken MN, Gupta R, Tsai JM, Sinha R, Corey D, *et al.* 2017 PD-1 expression by tumour-associated macrophages inhibits phagocytosis and tumour immunity. *Nature* **545** 495–499. (<https://doi.org/10.1038/nature22396>)

- Merseburger AS, Hammerer P, Rozet F, Roumeguère T, Caffo O, da Silva FC & Alcaraz A 2015 Androgen deprivation therapy in castrate-resistant prostate cancer: how important is GnRH agonist backbone therapy? *World Journal of Urology* **33** 1079–1085. (<https://doi.org/10.1007/s00345-014-1406-2>)
- Mok S, Koya RC, Tsui C, Xu J, Robert L, Wu L, Graeber T, West BL, Bollag G & Ribas A 2014 Inhibition of CSF-1 receptor improves the antitumor efficacy of adoptive cell transfer immunotherapy. *Cancer Research* **74** 153–161. (<https://doi.org/10.1158/0008-5472.CAN-13-1816>)
- Moughon DL, He H, Schokrpur S, Jiang ZK, Yaqoob M, David J, Lin C, Iruela-Arispe ML, Dorigo O & Wu L 2015 Macrophage blockade using CSF1R inhibitors reverses the vascular leakage underlying malignant ascites in late-stage epithelial ovarian cancer. *Cancer Research* **75** 4742–4752. (<https://doi.org/10.1158/0008-5472.CAN-14-3373>)
- Munder M, Schneider H, Luckner C, Giese T, Langhans C-D, Fuentes JM, Kropf P, Mueller I, Kolb A, Modolell M, *et al.* 2006 Suppression of T-cell functions by human granulocyte arginase. *Blood* **108** 1627–1634. (<https://doi.org/10.1182/blood-2006-11-010389>)
- Paller CJ & Antonarakis ES 2011 Cabazitaxel: a novel second-line treatment for metastatic castration-resistant prostate cancer. *Drug Design, Development and Therapy* **5** 117–124. (<https://doi.org/10.2147/DDDT.S13029>)
- Palmeri L, Vaglica M & Palmeri S 2008 Weekly docetaxel in the treatment of metastatic breast cancer. *Therapeutics and Clinical Risk Management* **4** 1047–1059. (<https://doi.org/10.2147/TCRM.S3397>)
- Petrylak DP 2003 Docetaxel for the treatment of hormone-refractory prostate cancer. *Reviews in Urology* **5** S14–S21.
- Petrylak DP, Tangen CM, Hussain MH, Lara PN Jr, Jones JA, Taplin ME, Burch PA, Berry D, Moynour C, Kohli M, *et al.* 2004 Docetaxel and estramustine compared with mitoxantrone and prednisone for advanced refractory prostate cancer. *New England Journal of Medicine* **351** 1513–1520. (<https://doi.org/10.1056/NEJMoa041318>)
- Priceman SJ, Sung JL, Shaposhnik Z, Burton JB, Torres-Collado AX, Moughon DL, Johnson M, Lusic AJ, Cohen DA, Iruela-Arispe ML, *et al.* 2010 Targeting distinct tumor-infiltrating myeloid cells by inhibiting CSF-1 receptor: combating tumor evasion of antiangiogenic therapy. *Blood* **115** 1461–1471. (<https://doi.org/10.1182/blood-2009-08-237412>)
- Rapidis A, Sarlis N, Lefebvre J-L & Kies M 2008 Docetaxel in the treatment of squamous cell carcinoma of the head and neck. *Therapeutics and Clinical Risk Management* **4** 865–886. (<https://doi.org/10.2147/TCRM.S3133>)
- Rodriguez PC, Quiceno DG, Zabaleta J, Ortiz B, Zea AH, Piazuolo MB, Delgado A, Correa P, Brayer J, Sotomayor EM, *et al.* 2004 Arginase I production in the tumor microenvironment by mature myeloid cells inhibits T-cell receptor expression and antigen-specific T-cell responses. *Cancer Research* **64** 5839–5849. (<https://doi.org/10.1158/0008-5472.CAN-04-0465>)
- Romanel A, Gasi Tandefelt D, Conteduca V, Jayaram A, Casiraghi N, Wetterskog D, Salvi S, Amadori D, Zafeiriou Z, Rescigno P, *et al.* 2015 Plasma AR and abiraterone-resistant prostate cancer. *Science Translational Medicine* **7** 312re310. (<https://doi.org/10.1126/scitranslmed.aac9511>)
- Ryan CJ, Smith MR, Fizazi K, Saad F, Mulders PF, Sternberg CN, Miller K, Logothetis CJ, Shore ND, Small EJ, *et al.* 2015 Abiraterone acetate plus prednisone versus placebo plus prednisone in chemotherapy-naive men with metastatic castration-resistant prostate cancer (COU-AA-302): final overall survival analysis of a randomised, double-blind, placebo-controlled phase 3 study. *Lancet Oncology* **16** 152–160. ([https://doi.org/10.1016/S1470-2045\(14\)71205-7](https://doi.org/10.1016/S1470-2045(14)71205-7))
- Schellhammer PF, Chodak G, Whitmore JB, Sims R, Frohlich MW & Kantoff PW 2013 Lower baseline prostate-specific antigen is associated with a greater overall survival benefit from sipuleucel-T in the Immunotherapy for Prostate Adenocarcinoma Treatment (IMPACT) trial. *Urology* **81** 1297–1302. (<https://doi.org/10.1016/j.urology.2013.01.061>)
- Scher HI, Fizazi K, Saad F, Taplin M-E, Sternberg CN, Miller K, de Wit R, Mulders P, Chi KN, Shore ND, *et al.* 2012 Increased survival with enzalutamide in prostate cancer after chemotherapy. *New England Journal of Medicine* **367** 1187–1197. (<https://doi.org/10.1056/NEJMoa1207506>)
- Siegel RL, Miller KD & Jemal A 2017 Cancer statistics, 2017. *CA: A Cancer Journal for Clinicians* **67** 7–30. (<https://doi.org/10.3322/caac.21387>)
- Silberstein JL, Taylor MN & Antonarakis ES 2016 Novel insights into molecular indicators of response and resistance to modern androgen-axis therapies in prostate cancer. *Current Urology Reports* **17** 29. (<https://doi.org/10.1007/s11934-016-0584-4>)
- Sweeney CJ, Chen Y-H, Carducci M, Liu G, Jarrard DF, Eisenberger M, Wong Y-N, Hahn N, Kohli M, Cooney MM, *et al.* 2015 Chemohormonal therapy in metastatic hormone-sensitive prostate cancer. *New England Journal of Medicine* **373** 737–746. (<https://doi.org/10.1056/NEJMoa1503747>)
- Tannock IF, de Wit R, Berry WR, Horti J, Pluzanska A, Chi KN, Oudard S, Theodore C, James ND, Turesson I, *et al.* 2004 Docetaxel plus prednisone or mitoxantrone plus prednisone for advanced prostate cancer. *New England Journal of Medicine* **351** 1502–1512. (<https://doi.org/10.1056/NEJMoa040720>)
- Tap WD, Wainberg ZA, Anthony SP, Ibrahim PN, Zhang C, Healey JH, Chmielowski B, Staddon AP, Cohn AL, Shapiro GI, *et al.* 2015 Structure-guided blockade of CSF1R kinase in tenosynovial giant-cell tumor. *New England Journal of Medicine* **373** 428–437. (<https://doi.org/10.1056/NEJMoa1411366>)
- Xu J, Escamilla J, Mok S, David J, Priceman S, West B, Bollag G, McBride W & Wu L 2013 CSF1R signaling blockade stanches tumor-infiltrating myeloid cells and improves the efficacy of radiotherapy in prostate cancer. *Cancer Research* **73** 2782–2794. (<https://doi.org/10.1158/0008-5472.CAN-12-3981>)

Received in final form 3 September 2018

Accepted 11 September 2018

Accepted Preprint published online 11 September 2018

RESEARCH ARTICLE

Establishment of xenografts of urological cancers on chicken chorioallantoic membrane (CAM) to study metastasis

Junhui Hu¹, Moe Ishihara¹, Arnold I. Chin^{2,4} and Lily Wu^{1,2,3,4,*}

¹Department of Molecular and Medical Pharmacology, ²Department of Urology, ³Department of Pediatrics, and ⁴Jonsson Comprehensive Cancer Center, David Geffen School of Medicine, University of California at Los Angeles, CA 90095, USA

*Correspondence: Lily Wu, lwu@mednet.ucla.edu

Abstract

Cancer of the urological system commonly occurs in the kidney, bladder, and prostate gland. The clear cell subtype of renal cell carcinoma (ccRCC) constitutes the great majority of kidney cancer. Metastatic ccRCC portends a very poor outcome with no effective treatment available. Prostate cancer is the most common cancer in males in the US. Despite recent advances in selective kinase inhibitors and immunotherapies, the rate of developing new treatment from bench to bedside is slow. A time-consuming step is at the animal drug testing stage, in which the mouse model is the gold standard. In the pursuit to streamline the *in vivo* cancer biology research and drug development, we explored the feasibility of the chicken chorioallantoic membrane (CAM) model to establish xenografts. The CAM model greatly shortens the time of tumor growth and lowers the cost comparing to immunocompromised mice. We generated CAM xenografts from ccRCC, bladder and prostate cancer, with established cancer cell lines and freshly isolated patient-derived tissues, either as primary tumor cells or small pieces of tumors. The successful CAM engraftment rate from the different tumor sources is 70% or above. Using our previously established metastatic ccRCC mouse model, we showed that the CAM xenograft maintains the same tumor growth pattern and metastatic behavior as observed in mice. Taken together, CAM can serve as a valuable platform to establish new patient-derived xenografts (PDXs) to study tumor biology, thus accelerating the development of individualized treatment to halt the deadly metastatic stage of cancer.

Key words: chorioallantoic membrane; prostate cancer; bladder cancer; kidney cancer; animal model

Received: 11 July 2019; Revised: 23 August 2019; Accepted: 26 August 2019

© The Author(s) 2019. Published by Oxford University Press on behalf of West China School of Medicine & West China Hospital of Sichuan University. This is an Open Access article distributed under the terms of the Creative Commons Attribution License (<http://creativecommons.org/licenses/by/4.0/>), which permits unrestricted reuse, distribution, and reproduction in any medium, provided the original work is properly cited.

Introduction

Urological malignancies frequently arise from the epithelial cells of the major organs, including the kidney, ureter, bladder, urethra, prostate, and testes¹. Prostate cancer is the most prevalent urological cancer in males in the US, estimated to have 174 650 newly diagnosed cases and 31 620 deaths in 2019². Bladder cancer is the sixth most common cancer in the US, as estimated 80 470 and 17 670, new cases and deaths, respectively in 2019². As major organs involved in excretory function, cancers of the bladder and kidney are heavily influenced by environmental and carcinogen exposures, such as tobacco smoking. Interestingly, both of these malignancies are 2 to 3 times more prevalent in men than women. Despite advances in surgical technology and drug development, the survival rate of bladder cancer remained unchanged from 2009 to 2015². The incidence of kidney cancer is slightly lower than bladder cancer in the US, with new cases and deaths in 2019 estimated to be 74 000 and 15 000, respectively. However, the incidence of kidney cancer is increasing in the last 20 years, from about 10 to 16.1 per 100 000 persons². The clear cell histological subtype of renal cell carcinoma (ccRCC) is the most common type of kidney cancer. Although organ-confined ccRCC has a favorable 5-year survival of 74.8%, approximately 30% of patients will develop a metastatic disease with a very poor 5-year survival of only 10%. Disseminated metastatic disease is the lethal stage for all solid tumors, including all these three urological cancers. Unfortunately, no effective anti-metastasis treatment is available at this time. Further investigation of the cancer biology and testing of new therapeutics in new patient-derived tumor models is sorely needed to propel the next wave of advancement for these urological cancers³⁻⁵.

The mouse model has been the gold standard for studying human diseases for several decades. The reasons for the popularity of mice include their small size, ease of colony expansion, their mammalian physiology, and most importantly, the advent of transgenic engineering technology to mimic human diseases⁶. However, mouse experimentations have several limitations. First, genetically modified immunodeficient mouse strains needed for establishing patient-derived xenografts (PDXs) are very costly; many of them cost over \$100 per animal. Subcutaneous heterotopic implantation is the preferred site of initial attempts of PDXs engraftment in mice, mainly due to its superficial location as the deeper location of urological organs is difficult to assess engraftment. However, the relatively poor blood supply in subcutaneous tissue can slow or prevent the engraftment process. Generally, the engraftment of new PDXs of urological cancer in mice will require at least 2 months. Tumor models established on the chorioallantoic membrane (CAM) of chicken embryo offers several advantageous over the mouse model. In general, each fertilized egg costs less than US \$2, which

is 1%-2% the cost of each immunocompromised mouse. The maximal time of tumor growth on CAM is 2 weeks. Moreover, the open window on the eggshell created to drop the CAM for tumor implantation also allows for direct visualization of tumor growth.

CAM is a transparent membrane that serves as the lining of allantois⁷ and extends from the ventral wall of the endodermal hind-gut of the chicken embryo⁸. The growth of this membrane starts from embryonic development day 3 in chickens⁸. It has known to provide rich vasculature and a rapidly expanding area. The use of chicken as an experimental model for cancer research initiated the era of molecular oncology. More than a century ago in 1911, Dr. Peyton Rous discovered Rous sarcoma virus (RSV) as the causative agent of chicken sarcoma⁹, and in the following year, Dr. James Murphy further demonstrated that rat sarcoma could be transplanted into the chick embryo¹⁰. Later in the 1930s, CAM was frequently used to cultivate vaccines, viruses, and bacteria^{11,12}. In the last few decades, CAM utilization correlated closely with the growth of angiogenesis research as CAM was shown to be a good substitute for more expensive and laborious angiogenesis assay in mammalian animals, such as the corneal pocket assay¹³⁻¹⁵. The application of CAM in cancer research gained traction in early 2000, coincided with the advancement in 3D and live cell and tissue imaging that can be directly applied to CAM tumor models. The use of CAM has continued to increase in the last decade as it has been shown to be a good growth platform for a wide range of cancer cell lines, such as ovarian cancer¹⁶, colon cancer¹⁷, sarcoma¹⁸, kidney cancer¹⁹, melanoma²⁰, multiple myeloma²¹ and cancer tissues from hepatocellular carcinoma²², sarcoma²³, melanoma²⁴, and ovarian adenocarcinoma²⁵.

Despite the prolific use of CAM in cancer research in recent years, few studies have assessed the ability to establish new PDXs of urological cancers from different sources of patient-derived cancer cells and tissues. Here we demonstrated that CAM PDXs can be established efficiently from pre-existing human cancer cell lines, and primary tumor cells and small tumor pieces freshly isolated from surgical samples of urological cancers. Metastasis is a frequent and deadly manifestation of ccRCC in the clinic. Here, we demonstrated that the growth and metastatic behavior of a murine ccRCC model we recently developed^{26,27} could be fully reproduced in the CAM model. Our results support that the CAM model could be a valuable alternative *in vivo* model to establish new PDXs and study the biology of urological cancers.

Methods and Materials

Antibodies, primers, cell lines, and reagents

Anti-FLAG antibody was purchased from eBioscience (Cat#14-6681-82), anti-panCK antibody from Biogenex (Cat#AM273-5 M), anti-VHL antibody from Abcam (Cat#ab140989), and anti-CK8/18 from Novus (Cat#NBP2-

44929). Murine ccRCC cell line RENCA and human ccRCC cell line ACHN, prostate cancer cell lines CWR22v1 and C4-2 were purchased from the American Type Culture Collection (ATCC) and maintained in RPMI-1640, supplemented with 10% fetal bovine serum and penicillin/Streptomycin at a working concentration of 100 U/mL. Murine prostate cancer cells Myc-CaP were purchased from ATCC and maintained in DMEM, supplemented with 10% fetal bovine serum and penicillin/Streptomycin at a working concentration of 100 U/mL. Human bladder cancer cell lines T24 and HT-1376 were kind gifts from Dr. Arnold I. Chin and Dr. Hanwei Zhang at UCLA and maintained in the same condition as RENCA cells.

Lentiviral plasmid encoding mStrawberry and EGFP, together with flag tag or HA, and plasmid encoding firefly luciferase were constructed based on pSicoR (Addgene, #11579), and lentivirus was packaged as mentioned previously in the report²⁶.

Human ccRCC and bladder cancer patient specimen

The collection of patient ccRCC and bladder cancer tissues was undertaken according to the protocol approved by the UCLA Institutional Review Board. Clinical data, such as age, gender, and Eastern Cooperative Oncology Group performance status (ECOG PS), and pathological data, such as tumor-node-metastasis stage, histologic subtype, and Fuhrman grade, were collected from these cases. All involved patients consented to participate in the study before surgery. All experiments were performed according to the approved guidelines, complying with the principles for the use of human tissues, as stated in the Declaration of Helsinki. This study was approved by the Institutional Review Board of UCLA, under protocol # IRB 11-001363.

Establishment of a primary cancer cell line from patient ccRCC tissues

Patient's ccRCC samples were mechanically digested by mincing and chopping, followed by chemical digestion with Liberase (Cat#5401119001, Sigma Aldrich) at a working concentration of 0.5 u/mL in RPMI-1640. The samples were incubated in Liberase for 1 hour at 37 °C in a rotary mixer. The digestion was halted by the addition of RPMI-1640 supplemented with 10% FBS, and cells were centrifuged at $300 \times g$ for 5 min to pellet. Red blood cell lysis was performed when necessary (Cat#555899, BD). Then the cells were cultured in a 15-cm dish with 20 mL of RPMI-1640 supplemented with 10% FBS and 100 u/mL Penicillin/Streptomycin.

CAM xenograft model from cells and tissues

All experiments performed in fertilized eggs and embryo before hatching do not require IACUC approval. The CAM xenograft model was established and studied according

to the previously published protocols^{28,29}. Briefly, freshly laid fertilized eggs were purchased (Rhode Island Red Rooster, AA Lab Eggs). After 7 days of pre-incubation at 37-38 °C and 55%-65% humidity, the CAM beneath the lateral side of the egg shell was separated and retracted from the shell and then the overlying shell was removed to form a window for tumor implantation^{28,29}. On embryonic developmental day 10, the pre-existing cancer cell lines and patient-tissue-derived primary cancer cell lines were implanted on the CAM at the concentration of 2×10^6 cells/egg suspended in diluted Matrigel (Cat# 356234, Corning, USA; 1:2 diluted in pre-cooled RPMI-1640).

Tumor growth was recorded every other day, starting on tumor day 3 (or developmental day 13). For CWR22Rv1 tumors, BLI was also performed to record tumor (developmental day 19). The procedures were described in our previous reports^{26,27}, except that 100 μ L luciferin reconstituted to 30 mg/ml in saline and applied directly over the tumor, and 10 μ L isoflurane were directly injected into the allantois with an insulin syringe. At the endpoint (developmental day 20), the embryos were euthanized by being placed on ice for 20 min. The CAM tumors were harvested for gross picture and histological analyses. Chicken blood and organs were also collected to detect metastasis.

For patient samples, tumor tissue was chopped into small chunks around 2-3 mm in diameter and put on the CAM. 200 μ L diluted Matrigel was added to cover the samples for short-term nourishment. Other steps were performed as mentioned above.

For the experiment using CAM model to assess RENCA tumor growth and metastasis, 21 fertilized eggs were randomly divided into 3 groups and were implanted with VHL-WT, VHL-KO or a 1:1 mixture of both cells at 2×10^6 cells/egg ($n = 7$ per group). The tumors and embryo blood were harvested at developmental day 20 and assessed by tumor weight and circulating tumor cells by flow cytometry or RT-PCR to detect mStrawberry+ or EGFP+ cells, respectively. Both VHL-WT and VHL-KO cells were also tagged by FLAG epitope to allow histological detection.

Analysis of distant metastasis of ccRCC in hatched chicken and mouse

All animal studies described here have been approved by IACUC, designated as UCLA Chancellor's Animal Research Committee (ARC). The chicken embryos bearing CAM tumors were allowed to hatch and grow for 2 weeks. The VHL-WT cells were tagged with HA epitope and the VHL-KO cells were tagged with FLAG epitope to facilitate histological detection. After euthanasia with isoflurane inhalation followed by cervical dislocation, the lungs were extracted and fixed in 4% paraformaldehyde for paraffin-wax embedding. The ARC 2017-102-01A protocol covered these chicken experiments. The methods of establishing orthotopic renal tumors have been described in previous studies^{26,27,30} and approved in the ARC 2002-049-53 protocol.

Flow cytometry and immunofluorescence staining

Flow cytometry was performed on chicken blood to detect circulating tumor cells, as described previously^{26,27}. Immunofluorescence staining was performed in the same way as immunohistochemical staining previously reported in our study²⁶, except for TSA staining. TSA kit (Cat# NEL756001KT, PerkinElmer) was used at a 1:200 dilution ratio for tertiary signal amplification of FLAG.

Statistics

Each experiment was performed at least in triplicates unless otherwise stated. Data are presented as mean \pm standard deviation (SD). Significance was determined by a paired Student's T-test when there were two groups or by a one-way ANOVA when there were three or more groups (GraphPad Prism ver6.0). A *p*-value cutoff of 0.05 was used for significance.

Results and Discussion

High-efficiency CAM engraftment with established renal, bladder and prostate cancer cell lines

The approach we have taken to establish CAM xenografts is illustrated in Fig. 1. In 2013, Fergelot *et al.* introduced human ccRCC cell lines RCC4, Caki-2 and 786-O into CAM and found that Caki-2 and 786-O formed tumors²⁸. Given the short 10 days of growth in CAM, we surmise that CAM could be more favorable to support the engraftment of the faster proliferative cell lines such as the murine RENCA ccRCC cell line, which has not been assessed in previous CAM studies. As shown in Fig. 2A and 2B, RENCA cells induced angiogenesis and grew to about 1 cm in diameter within 10 days. The cellular morphology of the CAM RENCA tumor was similar to mice tumor as assessed by H&E stain (Fig. 2C). The serial passage of CAM tumors had been reported previously²⁴. Here, we assessed whether CAM tumors could be passaged back in mice as a means to extend the tumor growth period. CAM RENCA tumor was re-transplanted into the subcutaneous tissue of nude mice and grew to a 1 cm diameter tumor in 3 weeks (Fig. 2D). The RENCA tumor cells were marked by the FLAG epitope. The RENCA CAM tumor before and after passaged back in mice showed a high degree of resemblance in cell morphology and FLAG expression as assessed by H&E and IHC stain, except that the chicken stroma and blood components (nucleated RBC) were replaced by the mouse counterparts (Fig. 2D, arrows). Next, we implanted the VHL-expressing human ccRCC cell line ACHN on CAM. ACHN cells established CAM xenografts consistently, but in smaller size than RENCA CAM tumors (Fig. 2E). The cell morphology of ACHN tumor engrafted in CAM and mouse was also similar (Fig. 2F). The tumor cells in the ACHN CAM tumor

were further confirmed to be of human origin by a human pan-cytokeratin stain (Fig. 2F, right panel).

In comparison to human kidney and prostate cancer, bladder cancer appears to be amenable to *in vitro* cultivation. This point is reflected by a high number of distinct bladder cancer cell lines reported in publications and the availability of 10 verified bladder cancer lines in reputable repositories. In contrast, there are only 5 to 6 established human prostate or kidney cancer cell lines that are widely used in research. The experience in CAM also supports the relative ease to establish CAM xenografts from a wide range of established bladder cancer cell lines. In 2007, Chin *et al.* established the CAM xenograft with the MGH line as an *in vivo* model for fluorescence diagnosis³¹. In the last 10 years, numerous studies have employed CAM xenograft from bladder cancer cell lines such as HT1197, 639 V, RT112, KU7, UMUC2, VM-CUB1, 5647, RT112 and T24 to investigate the involvement of different pathways such as CDK4/6, PI3K, AKT and *de novo* purine metabolism in bladder cancer progression^{5,32,33}. In our pilot studies, we found that both T24 and HT-1376 cells could establish xenografts consistently on CAM (Fig. 2G). The HT-1376 CAM tumors often grew more robustly with large proliferating tumor cells in comparison to T24 CAM tumors (Fig. 2G).

Chakravarthi *et al.* used DU145 prostate cancer CAM xenografts to evaluate the role of PAICS and *de novo* purine biosynthesis in prostate oncogenesis⁴. The increasing popularity of the CAM system is supported by the fact that 7 impactful studies in the last 2 years have incorporated the CAM model to augment the mouse model of prostate cancer to investigate a range of signaling pathways and microRNA that influence invasion and metastasis^{34–40}. From these recent studies, CAM xenografts have been established for all of the common human prostate cancer cell lines, including VCaP^{34,35}, CWR22Rv1³⁶, PC3^{37,38}, LNCaP³⁹, and PC-3 M-LN4⁴⁰. In this study, we also showed that CAM xenografts could be established with human prostate cancer cell line CWR22Rv1 and C4-2, as well as the murine Myc-CaP cell line without difficulty (Fig. 2H). The large cell and nuclear morphology of prostate cancer CAM xenografts, assessed by H&E stain, were consistent with proliferative cancer cells (Fig. 2I). We and many other investigators have popularized the use of sensitive *in vivo* bioluminescence imaging (BLI) to detect small volume or disseminated prostate cancer lesions^{41,42}. As shown in Fig. 2J, BLI can also detect growing CAM tumors, such as CWR22Rv1 cells that have been transduced with a firefly luciferase-expressing lentivirus.

CAM supports the efficient engraftment of ccRCC and bladder cancer patient-derived primary cancer cells and tumor tissues

Current molecular cancer research is heavily reliant on pre-existing cancer cell lines⁷. However, many of the commonly used cancer cell lines have been cultivated in

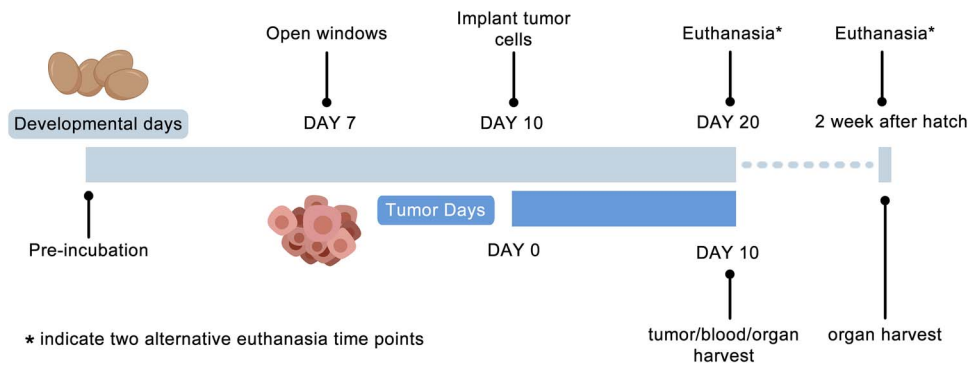


Figure 1. Schematic diagram of CAM xenograft implantation strategy.

petri dishes under *in vitro* growth conditions for decades. This long-term maintenance under artificial settings raises concern over whether these cancer cell lines can still represent human cancer, and more importantly, whether findings from these cancer lines are relevant to the clinical disease⁴³. Consequently, there is a strong demand to generate new primary cancer cell lines and xenografts from freshly harvested patient tumor tissues for discovery and investigative experiments⁴⁴. With this concern in mind, recent studies have utilized PDXs to evaluate responses to new therapies for kidney cancer⁴⁵. For instance, Sivanand *et al.* reported intrarenal implantation of 94 tumor surgical specimens that resulted in 16 stable patient-derived grafts to assess drug response⁴⁶. The engraftment rate of RCC PDXs in mice in recent reports is below 30%.

In the last 2 years, we have attempted to establish renewable sources of patient-derived tumor materials from a total of 10 cases of freshly harvested ccRCC surgical samples from a single urological surgeon, Dr. Arnold Chin. Our workflow included attempts to (i) cultivate primary tumor cell lines from dissociated tumor pieces, (ii) to directly implant small tumor pieces on CAM, and (iii) to implant established primary tumor cell lines on CAM. Table 1 summarizes the successful results. To generate primary cell lines, we disassociated tumor pieces to single cells. As a representative example (Fig. 3A), the first passage of cancer cells from one case displayed epithelial morphology and contained abundant lipid droplets in the cytoplasm, verified by the lipid Oil Red O stain (Fig. 3B). We were able to establish 5 primary cell lines from the 10 cases of ccRCC. These primary cell lines remained stable for at least 5 passages *in vitro*. The CAM tumor engraftment rate using the newly generated primary cells was very high, with a successful engraftment of 4 out of the 5 primary lines. A representative case of the primary ccRCC-derived CAM tumor was shown in duplicate in Fig. 3C. Direct visualization of CAM tumor growth from day 3 to 11 can inform on the tumor vascularization process. For instance, the Matrigel (white oval chunk) of CAM tumor #2 gained a pink hue from day 7 onward, coinciding with an increase of small capillaries emanating from the tumor over time. Histological examination of the CAM tumor revealed the co-existence of

cells of different sizes, as well as the majority of cells containing large nuclei, consistent with the characteristics of proliferating cancer cells (Fig. 3D).

Next, we assessed the feasibility of engrafting CAM xenografts from small pieces of fresh tumors (approximately 2 mm in diameter). Out of the 10 cases of ccRCC tumors we have attempted, the success rate of engrafting small fresh ccRCC tumor pieces was 70% (see Table 1). Figure 4A shows a representative case of CAM xenograft established from a fresh ccRCC tumor. Duplicate CAM xenografts from the same case were shown, with the left panels showing the xenografts *in situ* and the right showing the isolated xenograft with its associated CAM (Fig. 4A). A large nourishing artery can be seen coursing right of the tumor in #1, while the nourishing artery was coursing from below the CAM in tumor #2. Histological analyses of the patient's tumor tissue by anti-VHL (Fig. 4B) and H&E stain (Fig. 4C) revealed extensive intratumoral heterogeneity amongst the 4 areas (a, b, c, d) sampled in regards to cellular morphology as well as VHL expression. Those areas contained cells with an abundance of lipid in the cytoplasm and low level of VHL expression that representing the clear cell morphology (Fig. 4B and 4C). The CAM xenograft of this case contained tumor cells that resembled those located in areas c and d of the patient's tumor (Fig. 4C, right panel).

Bladder cancer is the second tumor type we attempted to establish primary cancer cell lines and PDXs on CAM. We have only collected fresh surgical samples of bladder cancer for 4 months as compared to over 2 years with RCC. Out of the 4 cases of surgical samples of bladder cancer harvested in the interim, we were unable to establish any primary cell lines using DMEM or RPMI-1640 media supplemented with fetal bovine serum. Previous reports have documented the need to supplement with additional growth factors, such as fibroblast growth factor (FGF)^{47,48}. At this juncture, we have not optimized the culturing conditions to establish a primary bladder cancer cell line. However, establishing bladder cancer PDXs on CAM from small pieces of a tumor had been straightforward, without needing any supplement. We were able to reproducibly generate CAM PDXs from all 4 out of 4 bladder cancer cases we collected. The engraftment of PDX on CAM from a representative case was

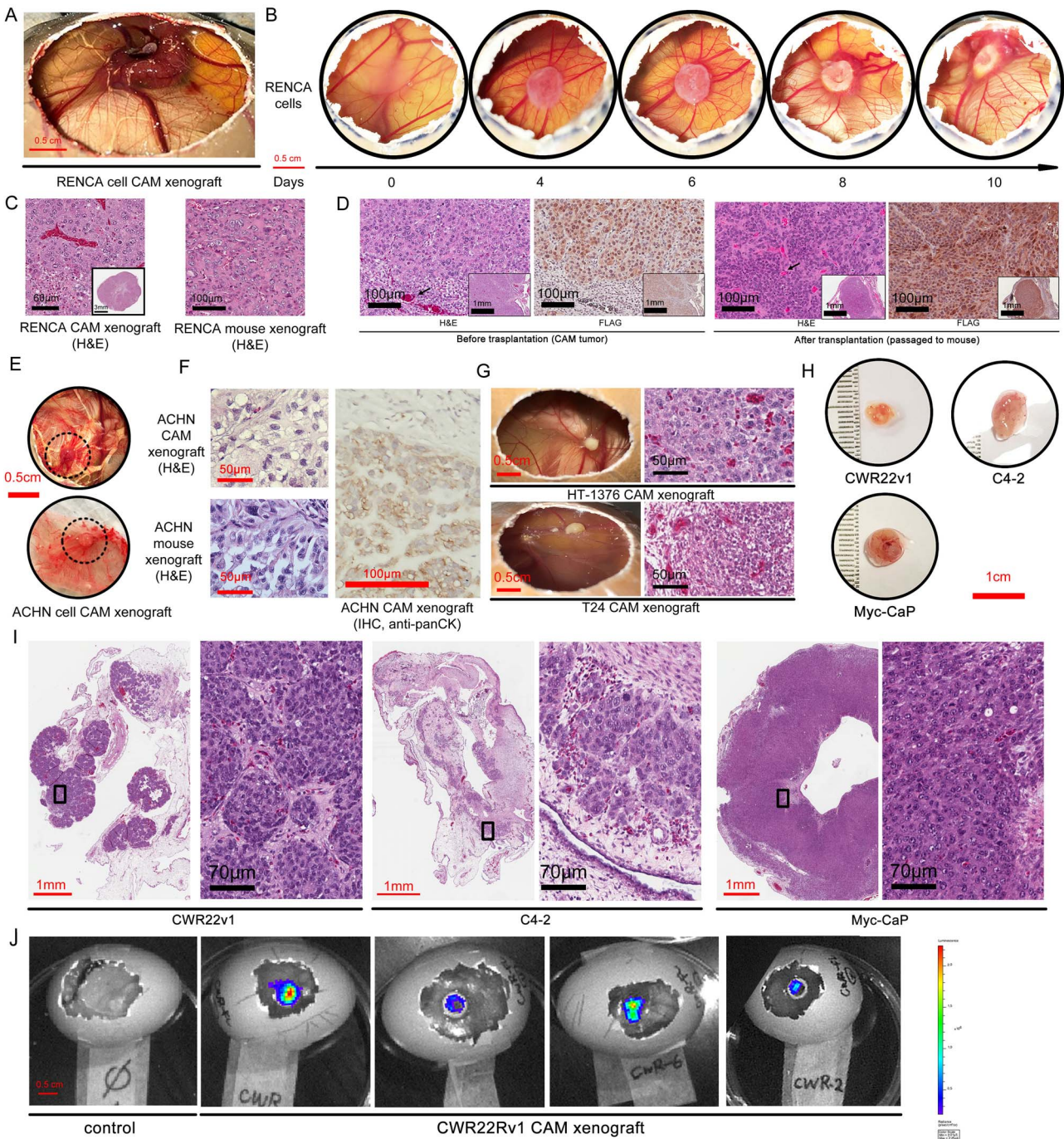


Figure 2. Establishment of CAM xenograft from pre-existing urological cancer cell lines. CAM tumor developed by implantation of 2×10^6 murine ccRCC RENCA cells. **A.** A gross view of CAM tumor on embryonic day 21. **B.** The development of the RENCA CAM tumor over the 10 days period after the implantation of the matrigel cell suspension. **C.** H&E stain of the RENCA CAM xenograft in parallel with the RENCA tumor established in the mouse kidney. **D.** H&E and FLAG IHC staining in both the RENCA CAM tumors and the CAM tumors re-transplanted subcutaneously in the nude mice. **E.** Gross view and **F.** H&E and anti-panCK IHC staining of CAM xenograft from human ccRCC cell line ACHN. Dash circled areas are tumors. **G.** Gross view of CAM xenograft and H&E stained tumor section from human bladder cancer cell line HT-1376 and T24. **H.** Gross view and **I.** H&E staining of CAM xenograft from human prostate cancer cell line CWR22Rv1 and C4-2, and murine prostate cancer cell line Myc-CaP. **J.** With lentiviral mediated transduction of firefly luciferase gene into CWR22Rv1 cells, their CAM xenograft can be visualized by bioluminescence imaging (BLI).

shown in triplicate in Fig. 4D. As an indication of tumor vascularization, the number of fine blood vessels coursing to and from the CAM tumor increased from day 3 to

day 11 after implantation (Fig. 4D). Moreover, the size of the CAM tumor grew from 2-3 mm in diameter at the time of implantation to about 5-7 mm in diameter on

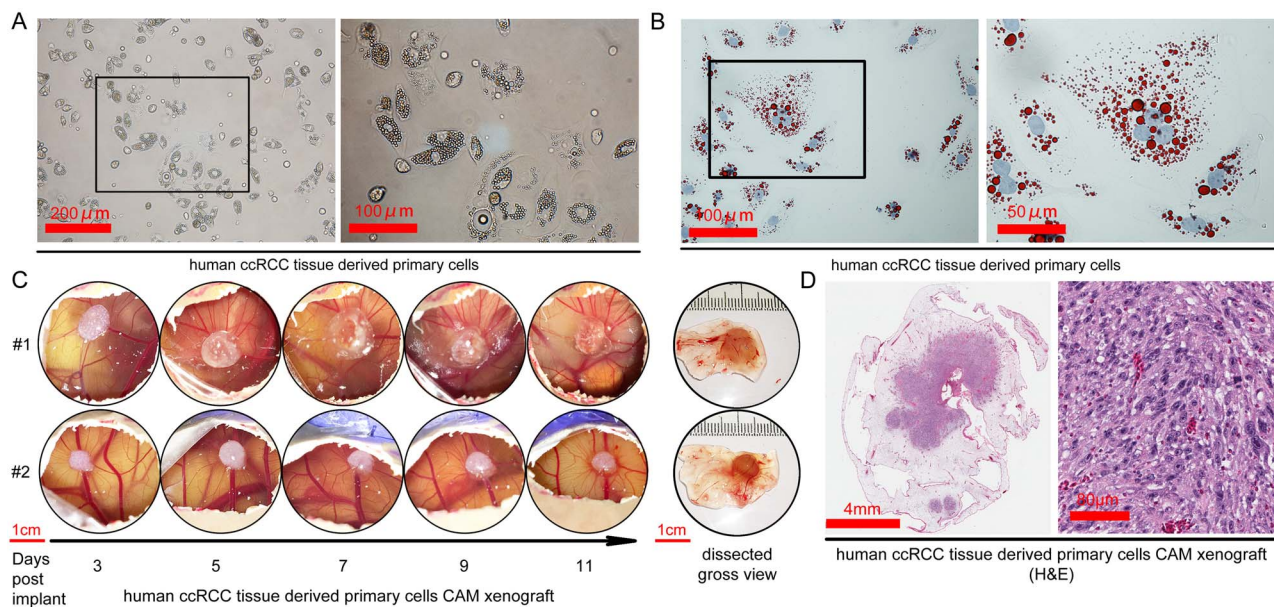


Figure 3. CAM can support engraftment of primary cancer cells derived from patient's ccRCC tumor. A. The morphology of primary cancer cells derived from freshly harvested patient ccRCC tumor under phase contrast microscope. B. Oil Red O stain of tumor cells. C. The development of the primary ccRCC-derived CAM tumor from day 3 to 11 after the implantation of early passage (within 10 passages) primary cells on CAM at 2×10^6 cells/egg. D. H&E stain of a CAM xenograft developed from primary ccRCC tumor cells.

day 11 (Fig. 4E). Histological examination revealed that the CAM tumor contained extensive fibrous tissues in conjunction with small foci of tumor cells that resemble the cellular morphology of the patient's bladder tumor (Fig. 4F). In the second case of slower growing bladder cancer PDXs, we used a human cytokeratin 8/18 IHC to identify the tumor cells (Fig. 4G).

PDXs engrafted directly from patients' tumors are extremely valuable sources of living tumor tissue for further investigation of cancer biology and pilot therapeutic studies. Although our current experience of establishing new CAM PDXs of ccRCC and bladder cancer is still quite limited in number, 10 and 4 cases, respectively, the success rate of CAM engraftment of 70%-100% is much higher than recently reported engraftment rate of PDX in mice^{45,46}. The high success rate could be attributed to the richness and naïve nature of the CAM vasculature that readily vascularizes the implanted tumor cells and tissues. Furthermore, the visible nature of CAM and its short growth period are very helpful in saving time and labor in the generation of PDXs. Here, we showed CAM PDXs retained some of the cellular morphology and histological features of patients' tumors. Confirmation that CAM PDX fully retains the characteristics of patients' tumors will require detailed genetic and expression profiling. We are actively pursuing this line of investigation. We have found that primary ccRCC cell line and CAM tumor generated as described here retained the same genetic mutations as the patient's tumor they were derived from (data not shown). The use of CAM PDXs as a platform to pursue a pilot therapeutic evaluation is extremely attractive, especially to fulfilling the tenet of personalized medicine. Although Vu et al.⁴⁹ demonstrated the fea-

sibility of nanoparticle-mediated drug delivery in CAM tumors, the short 10-12 day window of tumor growth and treatment on CAM would post a significant challenge to assess the traditional therapeutic endpoints such as tumor volume. We are actively investigating this critical topic.

CAM xenograft recapitulates the metastatic behavior of mouse ccRCC model

Metastasis to lungs is a frequent and deadly manifestation of ccRCC in the clinic. Unfortunately, the lack of clinically relevant spontaneous metastatic ccRCC models has slowed the understanding and the development of effective treatment for this disease. We created a novel metastatic ccRCC model by CRISPR-mediated VHL gene deletion in the murine RENCA line^{26,27}, and established the parental VHL wildtype (VHL-WT) and VHL knockout (VHL-KO) RENCA cells. We have observed that VHL deletion leads to epithelial-mesenchymal transition (EMT) of VHL-KO cells and dramatic slowing in proliferation *in vitro*^{26,27}. As shown in Fig. 5A, VHL-WT cells grew well after implanted into the kidney but did not produce metastasis in distant organs. Replicating their *in vitro* phenotype, the EMT+ VHL-KO cells grew poorly in the kidney (Fig. 5A). Strikingly, a 1:1 mix of VHL-WT and VHL-KO cell-implanted tumors not only grew well in the kidney, but also produced rampant metastasis in the lung and, to a lesser degree, in the liver (Fig. 5A). These results suggested that an intriguing cooperative mechanism of metastasis is at play, in which the poorly-proliferative EMT+ VHL-KO cells induce the metastatic potential of non-EMT VHL-WT cells^{26,27}.

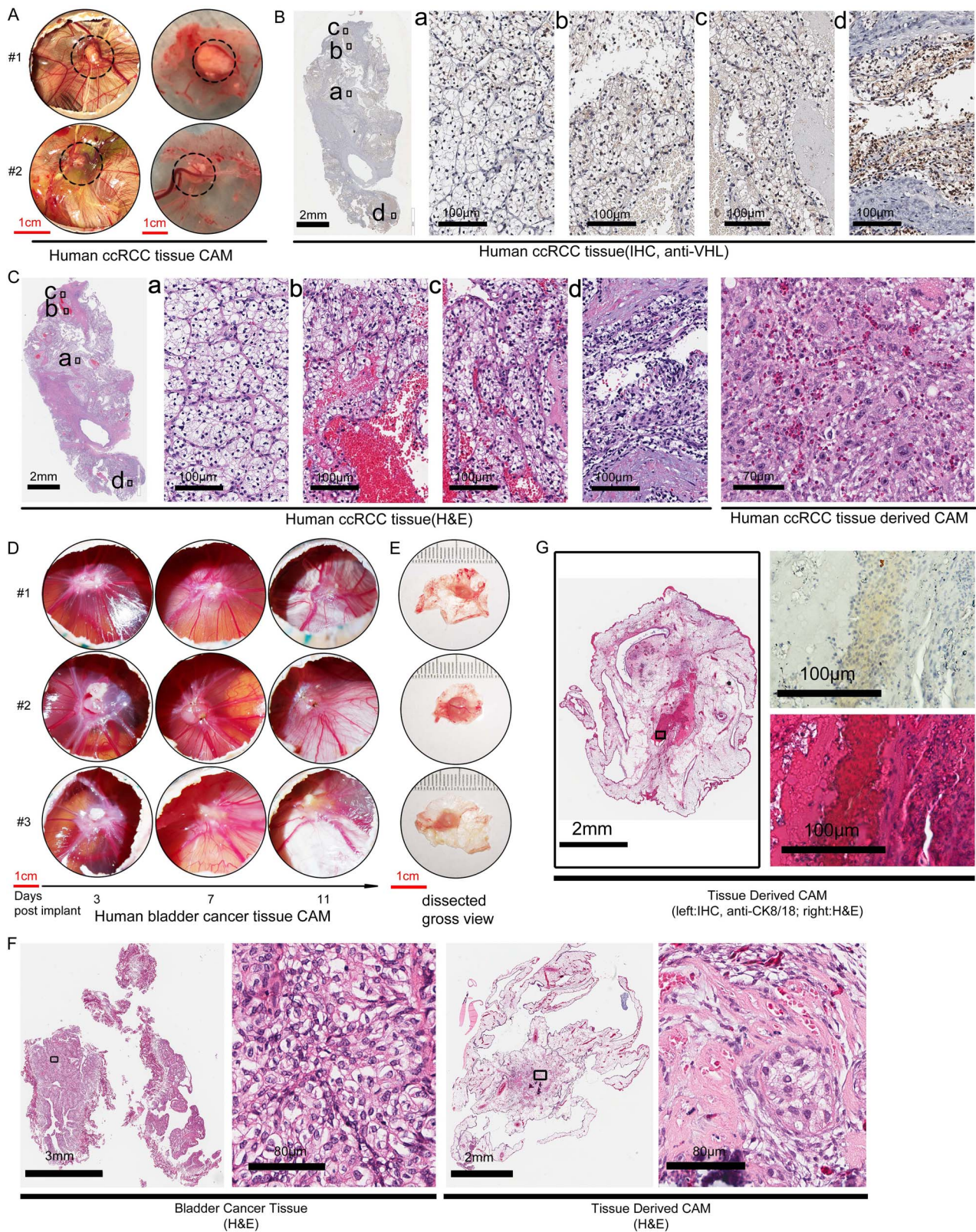


Figure 4. CAM ccRCC and bladder cancer xenografts derived from small pieces of patient's tumor. **A.** The gross view of a representative CAM xenograft established from small pieces of a surgical sample of human ccRCC tumor. Duplicate CAM tumors of the same case at embryonic day 20 (post fertilization) was shown. Left view: in situ CAM with tumor above and embryo below. Right view: isolated CAM with implanted tumor. Dash circled areas indicate tumors. **B.** The patient's original ccRCC tumor section assessed by anti-VHL IHC. **C.** H&E stain of patient's ccRCC tumor and the corresponding CAM tumor (right panels). **D.** CAM xenografts from a case human bladder cancer, viewed on 3, 7 and 11 days after implantation. Triplicate engraftment of the same case was shown. **E.** The gross view of dissected CAM bladder cancer xenograft from **D.** showed the tumor size has expanded from 2-3 mm at implantation to ~6 mm in diameter on day 11. **F.** H&E stain of the patient's bladder cancer tissue and the CAM PDX derived from it. Small foci within the CAM PDX retain cancer cell morphology similar to the patient's tumor. **G.** In a different case of bladder cancer from that shown in **D-F**, the CAM PDX established (left panel) were subject to anti-CK8/18 human cytokeratin IHC staining (right upper panel) to identify human epithelial cells within the PDX, with its corresponding H&E stain (right lower panel).

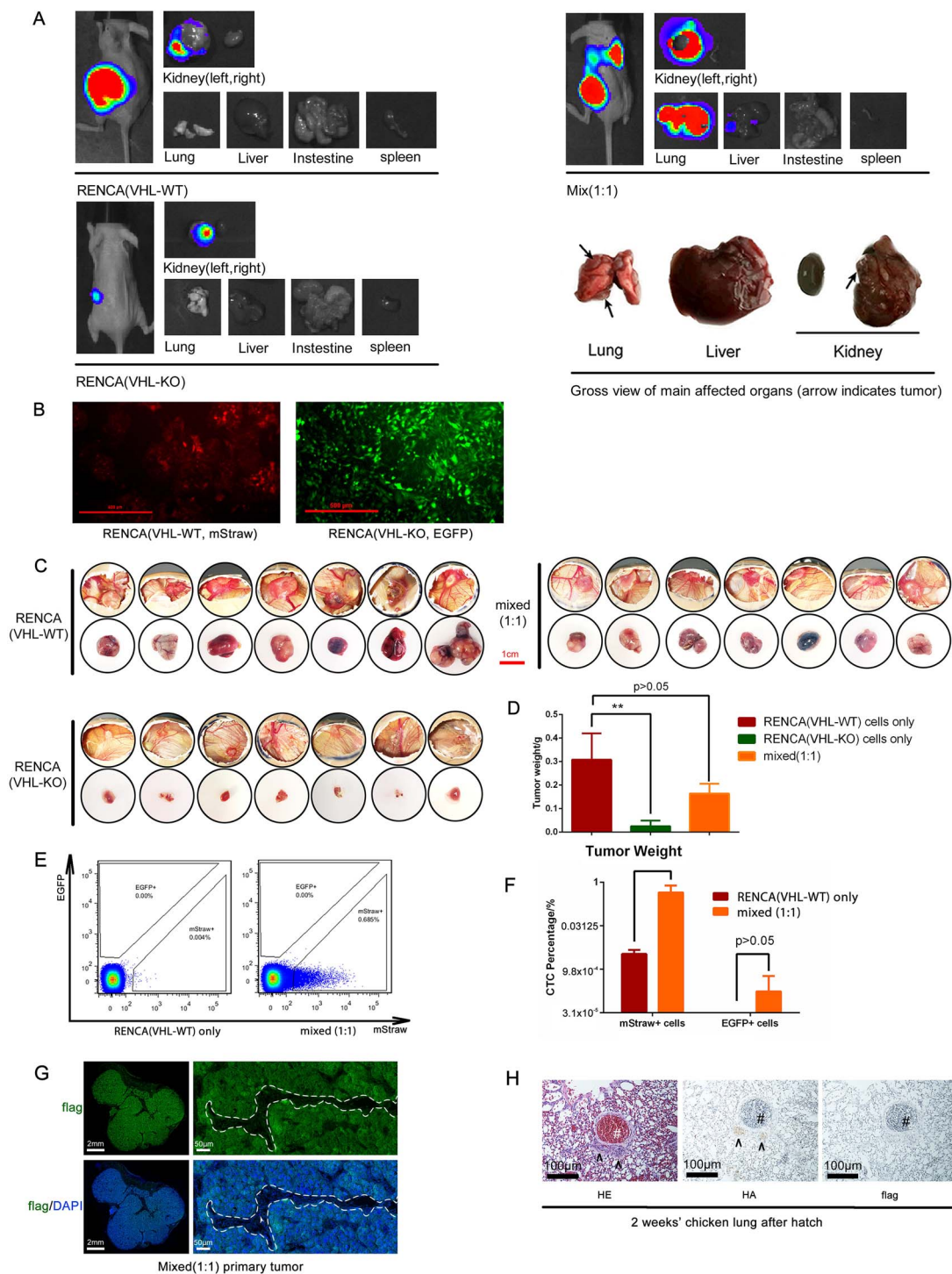


Figure 5. CAM xenografts recapitulate the metastatic behavior of an engineered murine ccRCC model. **A.** Mice were implanted orthotopically in the left kidney with either VHL wildtype (VHL-WT) RENCA cells, VHL knockout (VHL-KO) RENCA cells or a 1:1 mixture of both cells (with a total cell count of 2×10^6). At 4 weeks after tumor implantation, bioluminescence imaging (BLI) was performed on each group of mice and the major organs harvested from each mouse. The enlarged gross view of the organs in the mixed tumor bearing mouse was shown in right lower panel. **B.** Immunofluorescence staining of VHL-WT RENCA cells (labeled with mStrawberry) and VHL-KO cells (labeled with EGFP). **C.** The gross in situ views of CAM tumor and isolated CAM tumor from each group were shown ($n = 7$ per group). **D.** The average tumor weight of the 3 groups of CAM tumors was shown. **E.** Flow cytometric analysis of circulatory tumor cell showed that mixed CAM tumor produced more (mStrawberry+) cancer cells in the blood of chick embryo. **F.** RT-PCR analysis confirmed that VHL-WT (mStrawberry+) cells were the predominant circulating tumor cells. **G.** Immunofluorescence stain of the FLAG-tagged tumor cells (green) that invaded into vasculature. The CAM tumor cells (green) could be distinguished from avian stromal cells and nucleated red blood cells. The areas within the white dash line indicate the blood vessels and the white arrow indicates a nucleated chicken red blood cell. **H.** CAM tumors were established with a 1:1 mixed of VHL-WT cells (HA tagged) and VHL-KO cells (FLAG tagged) and embryos were allowed to hatch and grow for additional 2 weeks. Immunohistochemical analyses of lung sections from the 2-week old chick were shown. Arrows indicate two metastatic lesions in lung and # indicates a big blood vessel in the chicken. (**: $p < 0.01$)

Table 1. A summary of CAM xenograft engraftment from different cell or tissue sources of kidney, bladder or prostate cancer.

	Kidney cancer (ccRCC)	Bladder Cancer	Prostate Cancer
Cell line	RENCA, ACHN	HT-1376, T24	CWR22v1, C4-2, Myc-CaP
Primary tumor cells	YES, 4 out of 5 cases	Not yet tried*	Not yet tried
Tissue chunks	YES, 7 out of 10 cases	YES, 4 out of 4 cases	Not yet tried
Xenograft integrity	Good	Moderate, small foci of tumor with extensive fibroblasts	Good for cell lines
Advantages as compared to mouse model	<ol style="list-style-type: none"> 1. Shortened period of vascularization (~2 days) 2. Shortened period of overall tumor growth with comparable size 3. In general, CAM tumor with $\sim 2 \times 10^6$ tumor cells can grow to 1 cm in diameter in 10-11 days 4. Great saving in cost (~\$1 for each fertilized egg) in comparison to mouse (>\$100 for each immunocompromised mouse) 5. Tumor growth visible to naked eye 		
Disadvantages as compared to mouse model	<ol style="list-style-type: none"> 1. Difficult to achieve significant tumor expansion with slow growing tumor cells or tumor tissues in the short 10-11 days growth period allowed in CAM 2. Challenging to assess treatment response in 11 days 3. Difficult to detect metastasis in chick embryo organs due to the short time period of growth and different circulation pattern 		

*Unable to recover primary tumor cells from surgical tissues with RPMI-1640 or DMEM media supplemented with 10% FBS.

Here, we strive to assess whether the CAM xenograft can also recapitulate the growth and metastatic behavior of our VHL-KO and VHL-WT RENCA model^{26,27}. To facilitate the tracking of these two clonal purified cell lines *in vivo*, we marked them by lentiviral transduction, VHL-WT cells with the mStrawberry fluorescence protein and VHL-KO cells with the EGFP (Fig. 5B). These two cancer cell lines were also tagged with FLAG antigen to aid their identification by histological analyses. The CAM of 21 fertilized eggs were implanted with either VHL-WT cells only or VHL-KO cells only or a 1:1 mixture of these two ($n = 7$ per group). The growth rate of the CAM tumors was similar to their mouse counterparts²⁶ (Fig. 5A). The VHL-WT and mixed cell group of CAM tumors grew well, while the CAM tumors of VHL-KO group grew poorly. These findings were confirmed by measurement of tumor size (Fig. 5C) and weight (Fig. 5D). To assess tumor cell escape into circulation, the first intravasation step of metastasis, we analyzed circulatory tumor cells by flow cytometry. As shown in Fig. 5E and 5F, the presence of VHL-KO cells in the mixed tumor greatly enhanced the number of VHL-WT cells in circulation. Also, it confirms that the number of cancer cells that escaped into circulation in the mixed CAM tumor was much higher than that in the CAM tumors with VHL-WT cells only (Fig. 5E), and the majority of circulatory tumor cells was mStrawberry+VHL-WT RENCA cells (Fig. 5F). To examine the vascular invasion of tumor cells in the CAM xenograft, we used immunofluorescent staining with an anti-FLAG antibody to identify tumor cells at the tumor and vessel junction. Figure 5G shows the presence of tumor cells (FLAG+)

interspersed with chicken nucleated red blood cells (white arrow) within a blood vessel (demarcated by the dashed line).

Due to the short growth period on CAM before hatching and the decreased blood perfusion to the uninflated chicken embryo lung, detecting metastasis in the lungs of chicken embryo was expected to be very challenging. To overcome these limitations, we obtained approval from the Institutional Animal Care and Use Committee (IACUC) to extend the analyses of distant metastases in hatched chickens. In a separate experiment, we implanted a CAM tumor with 1:1 mixed VHL-WT and VHL-KO RENCA cells that were marked by HA-tag and flag-tag, respectively. The hatched chicks that bore CAM tumors were grown for 2 additional weeks before euthanasia and tissue analyses (Fig. 1). This time extension enabled the cancer cells to establish small metastatic nodules in the chicken lung, as visualized by H&E stain (Fig. 5H). A majority of the tumor cells in the metastatic lesion was the HA-tagged VHL-WT cells. The flag-tagged VHL-KO cells were difficult to locate (Fig. 5H). This finding is highly consistent with what we observed in the mouse model (data not shown). Importantly, the avian CAM tumor model can reproduce the preferential homing of ccRCC tumor cells to the lungs, which is observed in clinical disease and our mouse model⁵⁰.

In this study, we demonstrated that CAM is an efficient system to establish xenografts from either pre-existing cancer cell lines, primary cancer cell lines or small tumor pieces from patient-derived ccRCC or bladder tumors. Table 1 summarizes successful CAM

xenografts we have attempted in the last 2 years, as well as the advantages and disadvantages of CAM in comparison to the mouse model. The CAM tumor model is now well-accepted by the scientific research community, supported by the fact that the number of publications involving CAMs has increased 10 folds from 2000, and the findings are often published in the most prestigious journals^{5,24,51}. Given the high efficiency of PDXs engraftment on CAM in a short 10-day period, it holds great promise as an *in vivo* platform to pursue pilot drug screening on individual patient's tumor. Although many challenges remain unsolved to achieve the ultimate goal of precision individualized medicine with CAM, it is proven to be a convenient *in vivo* system to accelerate the discovery of critical molecular mechanism in cancer biology, such as the lethal metastatic disease.

Acknowledgments

This study was supported by National Cancer Institute/National Institutes of Health (Grant No. 1R21CA216770), UC Tobacco-related Disease Research Program (Grant No. 271R-0016), Department of Defense (Grant No. W81XWH-15-1-0256) and Cancer Research Coordinating Committee (Grant No. CRC15-380768) to L.W. UCLA institutional support grant support included: UCLA JCCC grant no. P30CA016042, and UCLA CTSI grant no. UL1TR001881 (to L.W.). We thank UCLA Translational Pathology Core Laboratory for the preparation of tumor samples.

Conflict of interest

No conflict of interest is disclosed.

References

- Obara W, Kato R, Kato Y, et al. Recent progress in immunotherapy for urological cancer. *Int J Urol* 2017;**24**(10): 735–42. doi: 10.1111/iju.13400.
- Howlander N, Noone AM, Krapcho M, et al. (eds). SEER Cancer Statistics Review, 1975–2016, National Cancer Institute. https://seer.cancer.gov/csr/1975_2016/, based on November 2018 SEER data submission, posted to the SEER web site. April 2019.
- Owens B. Kidney cancer. *Nature* 2016;**537**(7620):S97. doi: 10.1038/537S97a.
- Chakravarthi BV, Goswami MT, Pathi SS, et al. Expression and role of PAICS, a de novo purine biosynthetic gene in prostate cancer. *Prostate* 2017;**77**(1):10–21. doi: 10.1002/pros.23243.
- Sathe A, Koshy N, Schmid SC, et al. CDK4/6 inhibition controls proliferation of bladder cancer and transcription of RB1. *J Urol* 2016;**195**(3):771–9. doi: 10.1016/j.juro.2015.08.082.
- Thomas KR, Capecchi MR. Site-directed mutagenesis by gene targeting in mouse embryo-derived stem cells. *Cell* 1987;**51**(3):503–12. DOI:10.1016/0092-8674(87)90646-5.
- Nowak-Sliwinska P, Segura T, Iruela-Arispe ML. The chicken chorioallantoic membrane model in biology, medicine and bioengineering. *Angiogenesis* 2014;**17**(4): 779–804. doi:10.1007/s10456-014-9440-7.
- Gilbert SF. *Developmental Biology*. Sunderland, Mass: Sinauer Associates, 2003, 306–345.
- Rous P, Murphy JB. Tumor implantations in the developing embryo. Experiments with a transmissible sarcoma of the fowl. *J Amer Med Ass* 1911;**56**:741–2.
- Murphy JB. Transplantability of malignant tumors to embryos of a foreign species. *J Am Med Assoc* 1912;**59**:874.
- Goodpasture EW, Woodruff AM, Buddingh GJ. The cultivation of vaccine and other viruses in the chorioallantoic membrane of chick embryos. *Science* 1931;**74**(1919): 371–2. doi:10.1126/science.74.1919.371.
- Morrow G, Syverton JT, Stiles WW, et al. The growth of leptospira icterohemorrhagiae on the chorioallantoic membrane of the chick embryo. *Science* 1938;**88**(2286): 384–5. doi:10.1126/science.88.2286.384.
- Bagley DM, Waters D, Kong BM. Development of a 10-day chorioallantoic membrane vascular assay as an alternative to the Draize rabbit eye irritation test. *Food Chem Toxicol* 1994;**32**(12):1155–60. doi: 10.1016/0278-6915(94)90131-7.
- Ribatti D. Chorioallantoic membrane vasculature. In: *The Chick Embryo Chorioallantoic Membrane in the Study of Angiogenesis and Metastasis*. Dordrecht: Springer Netherlands, 2010, 1–15.
- Jedelská J, Strehlow B, Bakowsky U, et al. The chorioallantoic membrane assay is a promising *ex vivo* model system for the study of vascular anomalies. *In vivo* 2013;**27**(6):701–5.
- Lokman NA, Elder AS, Ricciardelli C, et al. Chick chorioallantoic membrane (CAM) assay as an *in vivo* model to study the effect of newly identified molecules on ovarian cancer invasion and metastasis. *Int J Mol Sci* 2012;**13**(8): 9959–70. doi:10.3390/ijms13089959.
- Subauste MC, Kupriyanova TA, Conn EM, et al. Evaluation of metastatic and angiogenic potentials of human colon carcinoma cells in chick embryo model systems. *Clin Exp Metastasis* 2009;**26**(8):1033–47. doi: 10.1007/s10585-009-9293-4.
- Kunz P, Schenker A, Sähr H, et al. Optimization of the chicken chorioallantoic membrane assay as reliable *in vivo* model for the analysis of osteosarcoma. *PloS One* 2019;**14**(4):e0215312. doi:10.1371/journal.pone.0215312.
- Ferician O, Cimpean AM, Avram S, et al. Endostatin effects on tumor cells and vascular network of human renal cell carcinoma implanted on chick embryo chorioallantoic membrane. *Anticancer Res* 2015;**35**(12):6521–8.
- Lugassy C, Torres-Munoz JE, Kleinman HK, et al. Overexpression of malignancy-associated laminins and laminin receptors by angiotropic human melanoma cells in a chick chorioallantoic membrane model. *J Cutan Pathol* 2009;**36**(12): 1237–43. doi: 10.1111/j.1600-0560.2009.01273.x.
- Ribatti D, De Falco G, Nico B, et al. *In vivo* time-course of the angiogenic response induced by multiple myeloma plasma cells in the chick embryo chorioallantoic membrane. *J Anat* 2003;**203**(3):323–8. doi:10.1046/j.1469-7580.2003.00220.x.
- Marzullo A, Vacca A, Roncali L, et al. Angiogenesis in hepatocellular carcinoma: An experimental study in the chick embryo chorioallantoic membrane. *Int J Oncol* 1998;**13**(1): 17–21. doi:10.3892/ijo.13.1.17.
- Sys GM, Lapeire L, Stevens N, et al. The *in ovo* CAM-assay as a xenograft model for sarcoma. *J Vis Exp* 2013;**2013**(77):e50522. doi: 10.3791/50522.
- Brooks PC, Montgomery AM, Rosenfeld M, et al. Integrin alpha v beta 3 antagonists promote tumor regression

- by inducing apoptosis of angiogenic blood vessels. *Cell* 1994;79(7):1157–64. doi:10.1016/0092-8674(94)90007-8.
25. Ismail MS, Torsten U, Dressler C, et al. Photodynamic therapy of malignant ovarian tumours cultivated on CAM. *Lasers Med Sci* 1999;14(2):91–96. DOI:10.1007/s101030050028.
 26. Hu J, Schokrpur S, Archang M, et al. A non-integrating Lentiviral approach overcomes Cas9-induced immune rejection to establish an Immunocompetent metastatic renal cancer model. *Mol Ther Methods Clin Dev* 2018;9:203–10. doi:10.1016/j.omtm.2018.02.009.
 27. Schokrpur S, Hu J, Moughon DL, et al. CRISPR-mediated VHL knockout generates an improved model for metastatic renal cell carcinoma. *Sci Rep* 2016;6:29032. doi:10.1038/srep29032.
 28. Fergelot P, Bernhard JC, Soulet F, et al. The experimental renal cell carcinoma model in the chick embryo. *Angiogenesis* 2013;16(1):181–194. doi:10.1007/s10456-012-9311-z.
 29. Palmer TD, Lewis J, Zijlstra A. Quantitative analysis of cancer metastasis using an avian embryo model. *J Vis Exp* 2011;2011(51):e2815. doi:10.3791/2815.
 30. Hu J, Guan W, Liu P, et al. Endoglin is essential for the maintenance of self-renewal and chemoresistance in renal cancer stem cells. *Stem Cell Reports* 2017;9(2):464–477. doi:10.1016/j.stemcr.2017.07.009.
 31. Chin WWL, Lau WKO, Bhuvanewari R, et al. Chlorin e6-polyvinylpyrrolidone as a fluorescent marker for fluorescence diagnosis of human bladder cancer implanted on the chick chorioallantoic membrane model. *Cancer Lett* 2007;245(1):127–33. doi:10.1016/j.canlet.2005.12.041.
 32. Sathe A, Guerth F, Cronauer MV, et al. Mutant PIK3CA controls DUSP1-dependent ERK 1/2 activity to confer response to AKT target therapy. *Br J Cancer* 2014;111:2103–13. doi:10.1038/bjc.2014.534.
 33. Sathe A, Chalaud G, Oppolzer I, et al. Parallel PI3K, AKT and mTOR inhibition is required to control feedback loops that limit tumor therapy. *PloS One* 2018;13(1):e0190854. doi:10.1371/journal.pone.0190854.
 34. San Martin R, Pathak R, Jain A, et al. Tenascin-C and integrin $\alpha 9$ mediate interactions of prostate cancer with the bone microenvironment. *Cancer Res* 2017;77(21):5977–88. doi:10.1158/0008-5472.CAN-17-0064.
 35. Civenni G, Albino D, Shinde D, et al. Transcriptional reprogramming and novel therapeutic approaches for targeting prostate cancer stem cells. *Front Oncol* 2019;9:385. doi:10.3389/fonc.2019.00385.
 36. Mesci A, Lucien F, Huang X, et al. RSPO3 is a prognostic biomarker and mediator of invasiveness in prostate cancer. *J Transl Med* 2019;17(1):125. doi:10.1186/s12967-019-1878-3.
 37. Shimada K, Nakamura M, Ishida E, et al. Prostate cancer antigen-1 contributes to cell survival and invasion through discoidin receptor 1 in human prostate cancer. *Cancer Sci* 2008;99(1):39–45. doi:10.1111/j.1349-7006.2007.00655.x.
 38. El Gaafary M, Buchele B, Syrovets T, et al. An alpha-acetoxytirucallic acid isomer inhibits Akt/mTOR signaling and induces oxidative stress in prostate cancer cells. *J Pharmacol Exp Ther* 2015;352(1):33–42. doi:10.1124/jpet.114.217323.
 39. Reuter A, Sckell A, Brandenburg LO, et al. Overexpression of microRNA-1 in prostate cancer cells modulates the blood vessel system of an in vivo hen's egg test-chorioallantoic membrane model. *In vivo* 2019;33(1):41–46. doi:10.21873/invivo.11436.
 40. Kim Y, Williams KC, Gavin CT, et al. Quantification of cancer cell extravasation in vivo. *Nat Protoc* 2016;11:937–48. doi:10.1038/nprot.2016.050.
 41. Adams JY, Johnson M, Sato M, et al. Visualization of advanced human prostate cancer lesions in living mice by a targeted gene transfer vector and optical imaging. *Nat Med* 2002;8(8):891–7. doi:10.1038/nm743.
 42. Jiang ZK, Sato M, Wei LH, et al. Androgen-independent molecular imaging vectors to detect castration-resistant and metastatic prostate cancer. *Cancer Res* 2011;71(19):6250–60. doi:10.1158/0008-5472.CAN-11-1520.
 43. Gillet J-P, Varma S, Gottesman MM. The clinical relevance of cancer cell lines. *J Natl Cancer Inst* 2013;105(7):452–8. doi:10.1093/jnci/djt007.
 44. Lalmahomed ZS, Coebergh van den Braak RRJ, Oomen MHA, et al. Multicenter fresh frozen tissue sampling in colorectal cancer: Does the quality meet the standards for state of the art biomarker research? *Cell Tissue Bank* 2017;18(3):425–31. doi:10.1007/s10561-017-9613-x.
 45. Patel A, Cohen S, Moret R, et al. Patient-derived xenograft models to optimize kidney cancer therapies. *Transl Androl Urol* 2019;8(Suppl 2):S156–65. doi:10.21037/tau.2018.11.04.
 46. Sivanand S, Pena-Llopis S, Zhao H, et al. A validated tumor-graft model reveals activity of dovitinib against renal cell carcinoma. *Sci Transl Med* 2012;4(137):137ra175. doi:10.1126/scitranslmed.3003643.
 47. Ito H, Yamaguchi K, Kotake T, Matsuzaki O. Primary culture of human bladder carcinomas and establishment of human bladder carcinoma cell line by serum-free culture. *Nihon Hinyokika Gakkai zasshi* 1989;80(12):1749–54. doi:10.5980/jpnjurol1989.80.1749.
 48. Roberson KM, Yancey DR, Padilla-Nash H, et al. Isolation and characterization of a novel human bladder cancer cell line: BK10. *In Vitro Cell Dev Biol Anim* 1998;34(7):537–44. doi:10.1007/s11626-998-0113-y.
 49. Vu BT, Shahin SA, Croissant J, et al. Chick chorioallantoic membrane assay as an in vivo model to study the effect of nanoparticle-based anticancer drugs in ovarian cancer. *Sci Rep* 2018;8(1):8524. doi:10.1038/s41598-018-25573-8.
 50. Bianchi M, Sun M, Jeldres C, et al. Distribution of metastatic sites in renal cell carcinoma: A population-based analysis. *Ann Oncol* 2012;23(4):973–80. doi:10.1093/annonc/mdr362.
 51. Ngan E, Stoletov K, Smith HW, et al. LPP is a Src substrate required for invadopodia formation and efficient breast cancer lung metastasis. *Nat Commun* 2017;8:15059. doi:10.1038/ncomms15059.